Elsevier Editorial System(tm) for Ceramics International
Manuscript Draft

Manuscript Number: CERI-D-14-03417R1

Title: Consolidation of different Hydroxyapatite powders by SPS: optimization of the sintering conditions and characterization of the obtained bulk products

Article Type: Full Length Article

Keywords: Hydroxyapatite; Tri-Calcium Phosphate (TCP), Spark Plasma Sintering; Mechanical properties

Corresponding Author: Dr. Roberto Orru, PhD

Corresponding Author's Institution: University of Cagliari

First Author: Alessio Cuccu, PhD Student

Order of Authors: Alessio Cuccu, PhD Student; Selena Montinaro, PhD; Roberto Orru, PhD; Giacomo Cao, PhD; Devis Bellucci, PhD; Antonella Sola; Valeria Cannillo, PhD

Abstract: The difference in purity, particle size, microstructure, and thermo-chemical stability of three commercially available hydroxyapatite powders are found to play an important role during their consolidation using Spark Plasma Sintering (SPS) as well as strongly affect the characteristics of the resulting sintered bodies. A fully dense material without secondary phases was obtained by SPS at 900°C, when using the relatively small sized, with refined grains and high purity powders. The sintered product, consisting of sub-micrometer sized hydroxyapatite grains, displayed optical transparency and good mechanical properties.In contrast, the higher temperature levels (up to 1200 °C) needed to sinter powders with larger particles, or finer ones which contain additional phases, lead to products with coarser microstructures and/or significant amount of β-TCP as a result of HAp decomposition. Optical characteristics, hardness and elastic modulus of the resulting sintered samples are correspondingly worsened.

Replies to the Reviewer's comments

First of all we would like to thank the Reviewer for considering our manuscript very good and the related conclusions interesting.

As suggested by the Reviewer, the comparison of the transformation temperatures from HAp to beta-TCP of the commercial powders considered in the present work with those ones indicated in the literature is reported in the revised version of the manuscript along with the corresponding sources.

Consolidation of different Hydroxyapatite powders by SPS: optimization of the sintering conditions and characterization of the obtained bulk products

A. Cuccu[1], S. Montinaro[1], R. Orrù[1,*], G. Cao[1] , D. Bellucci[2], A. Sola[2], V. Cannillo[2]

[1]*Dipartimento di Ingegneria Meccanica, Chimica e dei Materiali, Unità di Ricerca del Consorzio Interuniversitario Nazionale per la Scienza e Tecnologia dei Materiali (INSTM) - Università degli Studi di Cagliari, via Marengo 2, 09123 Cagliari, Italy*

[2]*Dipartimento di Ingegneria "Enzo Ferrari", Università degli Studi di Modena e Reggio Emilia, Via Vignolese 905, 41125 Modena, Italy*

* Author to whom correspondence should be addressed:

R. Orrù (E-mail: roberto.orru@dimcm.unica.it; Ph.: +39-070-6755076; Fax: +39-070-6755057), *Università degli Studi di Cagliari, via Marengo 2, 09123 Cagliari, Italy*

Revised Version

August 2014

Abstract

The difference in purity, particle size, microstructure, and thermo-chemical stability of three commercially available hydroxyapatite powders are found to play an important role during their consolidation using Spark Plasma Sintering (SPS) as well as strongly affect the characteristics of the resulting sintered bodies. A fully dense material without secondary phases was obtained by SPS at 900°C, when using the relatively small sized, with refined grains and high purity powders. The sintered product, consisting of sub-micrometer sized hydroxyapatite grains, displayed optical transparency and good mechanical properties.

In contrast, the higher temperature levels (up to 1200 °C) needed to sinter powders with larger particles, or finer ones which contain additional phases, lead to products with coarser microstructures and/or significant amount of β-TCP as a result of HAp decomposition. Optical characteristics, hardness and elastic modulus of the resulting sintered samples are correspondingly worsened.

Keywords: Hydroxyapatite; Tri-Calcium Phosphate (TCP), Spark Plasma Sintering; Mechanical properties

1. Introduction

Since hydroxyapatite ($Ca_{10}(PO_4)_6(OH)_2$), often referred to as HAp or HA, represents the main inorganic component of hard human tissues (bones and teeth), it is not surprising that it is regarded as one of the most investigated ceramics for biomedical application in either bulk form or as coating **[1-3]**.

Due to its importance, a large number of research studies addressed to the fabrication of bulk HAp products using pressureless and pressure-assisted sintering methods, mainly conventional Hot Pressing (HP) or innovative Spark Plasma Sintering (SPS) techniques, have been conducted so far **[2].**

It is well known that one of the main concerns accompanying heat processing of HAp is related to its thermochemical instability **[4]**. Indeed, HAp decomposition takes place when relatively high temperature conditions are encountered during powder consolidation. Correspondingly, negative effects on mechanical and biological characteristics of the resulting materials are often produced.

In this context, the SPS technology offers a suitable method for obtaining bulk ceramic products under relatively milder sintering conditions **[5]**. Indeed, the electric pulsed current flowing directly through the die containing the non-conductive HAp powders permits sample heating at higher rates and in shorter processing times with respect to conventional HP, where external elements are employed as heating source.

Along these lines, several studies have been conducted in the literature in the last decade for the fabrication of dense HAp ceramics by SPS **[6-19]**. Most of them take advantage of the SPS technology for the consolidation of previously synthesized lab-made **[6,8-11,13-15,17,19]** or commercial **[7,10,16,18-19]** HAp powders. Alternatively, one attempt to synthesize and simultaneously densify the HAp by reactive SPS was carried out starting from $CaHPO_4 \cdot 2H_2O$ and $Ca(OH)_2$ as reaction promoters **[12]**.

As a consequence of the different starting materials, the operating conditions (i.e. holding temperature, heating rate, applied pressure and dwell time) adopted in these studies to obtain nearly full dense HAp-based bodies vary in a quite wide range, i.e. 700-1200°C. However, the potential benefits deriving from the use of SPS are confirmed. In this regard, it is clear that the characteristics of the initial powders deeply affect the final composition as well as the resulting mechanical and biological properties of the sintered material. Indeed, the decomposition of HAp to produce Tri-Calcium Phosphate (TCP) **[8,11,15]** could not be associated only to the more drastic SPS conditions correspondingly adopted. For instance, no additional phases other than HAp were found in the 99.7% dense material fabricated in 10 min by SPS at 1200°C **[9]**. On the other hand, the presence of β-TCP was evidenced by **Lee et al. [11]** in the 96.4% dense material obtained when the sintering process was conducted at 1000°C for 2 min. The use of different SPS apparatuses and sample configurations might also play a role in this regard.

In order to systematically investigate the influence of the characteristics of the initial powders on the final composition as well as the resulting mechanical properties, in the present work bulk HAp ceramics are produced by SPS using three different commercially available powders. The starting materials are first characterized by laser scattering analysis, X-ray diffraction (XRD), SEM, heat treatments in air and thermogravimetric analysis in order to highlight their main differences (purity, particle and crystallite size, thermochemical stability, etc.). Each HAp powder is then consolidated by SPS. In particular, a systematic investigation is performed to identify the optimal sintering temperatures to obtain fully dense products, while keeping all the other parameters unchanged (SPS equipment, applied pressure, heating rate, holding time, sample configuration). The resulting optimal samples are compared from the compositional, microstructural and mechanical point of view.

2. Experimental materials and methods

The main characteristics, as provided by the vendors, of the three different commercial powders investigated in this work for the fabrication of dense HAp products are reported in **Table 1**. A more detailed particle size analysis was carried out in the present study taking advantage of a laser light scattering analyser (CILAS 1180, France). The starting powders were also examined by XRD using a Philips PW 1830 X-rays diffractometer equipped with a Ni filtered Cu K_{α} radiation (λ=1.5405 Å). The powders' morphology was investigated by scanning electron microscopy (SEM, mod. S4000, Hitachi, Japan).

The thermal stability of the HAp powders was studied by heat treating the raw materials in air environment at different temperatures, in the range of 700-1250°C, using a laboratory furnace (Nabertherm, mod. N60/ER, Germany). In addition, a thermogravimetric analysis (TGA) under non-isothermal conditions was carried out by slowly heating (10°C/min) the initial powders from room temperature to 1450°C using a NETZSCH STA 409PC Simultaneous DTA-TGA Instrument in presence of 100 mL/min air flow.

The HAp powders were sintered in the form of cylindrical disks (about 15 mm diameter, 3 mm thickness) by Spark Plasma Sintering (SPS 515S model, Sumitomo Coal Mining Co Ltd) under vacuum conditions (20 Pa). This apparatus is based on the combination of a uniaxial press (50 kN) with a DC pulsed current generator (10 V, 1500 A, 300 Hz), thus simultaneously providing a pulsed electric current through the sample (when electrically conductive) and the graphite container, along with a mechanical pressure through the punches. The pulse cycle was set to 12 ms on and 2 ms off, being the characteristic time of single pulse equal to about 3.3 ms. Both the die and the plungers were made of AT101 graphite (Atal s.r.l., Italy). The powders to be sintered (about 1.6 g) were poured inside a cylindrical graphite die with outside diameter of 35 mm, inside diameter of 15 mm, and 30 mm high. To protect the die/plungers and make sample release easier after sintering, the compact was lined with a graphite foil (0.13 mm thick, Alfa Aesar Karlsruhe, Germany). In addition, the die was surrounded by a layer of graphite felt (3 mm thick, Atal s.r.l., Italy) for thermal insulation purpose.

The most important SPS parameters, i.e. temperature, current, voltage between the machine electrodes, mechanical load and vertical sample displacement, were recorded in real time. The displacement output provides an indication of the evolution of the powders' densification during SPS. However, the thermal expansion of sample, electrodes, graphite blocks, spacers and plungers is also responsible for the measured value. All these contributions, but that of the sample, can be separately accounted for by following a specific procedure **[20]**, thus obtaining the sample shrinkage (δ), which will be considered in what follows. In any case, the final consolidation level was determined by measuring the density of the samples obtained at the end of the SPS process. After sintering, the electric current was turned off, the mechanical load released, the sample allowed to cool to room temperature and then removed from the die. For the sake of reproducibility, each experiment was repeated at least twice.

SPS experiments were conducted under temperature controlled mode using a K-type thermocouple (Omega Engineering Inc., USA) inserted inside a small hole drilled near the center of the external surface of the graphite die. Temperature levels were also measured by means of an infrared pyrometer (CHINO, mod. IR-AHS2, Japan) focused on the lateral surface of the graphite mould.

The effect of the dwell temperature, T_D, on the product characteristics was investigated by performing all SPS experiments at constant values of the holding time (t_D=5 min), the mechanical pressure (P=30 MPa), and the heating rate (75°C/min), to achieve the desired value from the room temperature.

Relative densities were determined by the Archimedes' method after accurately polishing SPSed products and considering 3.16 g/cm^3 as theoretical value.

The microstructure of the optimal SPSed products was examined by SEM. To this aim, the sintered specimens were first mirror polished and then chemically etched for 10 s using a 3 vol.% HNO_3 solution.

The selected samples were also investigated from a mechanical point of view. A depth-sensing indentation technique was applied to determine the local elastic modulus and Vickers micro-hardness. With this aim, the samples were cut, mounted in resin and polished according to a standard metallographic procedure. The indentations were performed using an OpenPlatform instrument (CSM Instruments, Peseux, Switzerland), equipped with a Vickers indenter tip. For each sample, two different loading conditions were considered:

- low load: maximum applied load: 0.50 N; loading/unloading rate: 0.75 N/min; loading time: 15 s;
- high load: maximum applied load: 2.00 N; loading/unloading rate: 3.00 N/min; loading time: 15 s.

For statistical purposes, 30 indentations were performed for each sample and for each loading condition. For each indentation, the load-penetration depth curve was automatically acquired and then analyzed according to the Oliver and Pharr method to evaluate the local elastic properties **[21]**.

3. Results and discussion

3.1 Characterization of initial powders

The results related to the granulometry of the three different types of powders measured by laser light scattering analysis are summarized in **Table 2**. While **HAp_1** and **HAp_2** systems display similar fine particles, **HAp_3** powders are relatively coarser. This feature is clearly confirmed when examining the corresponding SEM micrographs (**Figure 1**). Specifically, both **HAp_1** and **HAp_2** materials generally consist of micrometer-sized aggregates made of sub-micrometer grains. In contrast, the **HAp_3** product exhibits coarser particles, up to 100 μm sized, characterized by a sponge like structure with pores down to 100 nm (**Figure 1(f)**).

The comparison of the corresponding XRD patterns is shown in **Figure 2**. On the basis of this analysis it is possible to state that HAp is the only phase present in **HAp_2** and **HAp_3**, while a non-negligible amount of $CaHPO_4$ was detected in **HAp_1** powders. In addition, the **HAp_1** and **HAp_2** systems displayed relatively broad diffraction peaks, to indicate their finer microstructure, in contrast to the narrow peaks observed when considering the **HAp_3** material.

The thermal stability of the starting powders was first evaluated by heat-treating the different raw materials in a furnace under air environment. The XRD spectra of the heat-treated powders are reported in **Figures 3(a)-(c)**.

No additional phases were detected by XRD when the **HAp_1** system was heat-treated at temperatures equal or lower than 700°C. On the other hand, as the temperature was raised to 750°C, the β-TCP phase (rhombohedral lattice) appeared in the XRD pattern of the end product. In addition, as higher thermal levels were achieved, the decomposition of HAp was found to increase progressively. Specifically, β-TCP becomes the major crystalline constituent in powders heat treated at 900°C, while only minor amounts of HAp and $CaHPO_4$ are present.

On the other hand, as evidenced in **Figures 3(b)** and **3(c)**, no secondary species are found in XRD patterns of **HAp_2** and **HAp_3** powders heat-treated up to 1250°C. The most significant change, particularly for **HAp_2**, is represented by a certain peak narrowing, with respect to the original material, thus indicating that grain growth is induced by the heat treatment.

In order to overcome the temperature limitation (1300°C) of the furnace utilized in the previous heat-treatment as well as to obtain further information regarding the chemico-physical stability of the powders under consideration, the latter ones have been also characterized by TGA up to 1450°C. The corresponding mass losses as a function of the temperature are plotted in **Figure 4** for the three systems. It is possible to observe that only for temperatures above 1000°C the **HAp_3** material significantly changes its mass. In contrast, the curves corresponding to the other two products markedly decrease just after the TGA test starts. Moreover, the weight losses resulting at the end of the experiment for **HAp_1** and **HAp_2** are 3-4 times higher than the value obtained when processing the **HAp_3** material.

The mass loss profiles described above can be associated to the compositional changes taking place in the powders as the temperature increases during the TGA test. This information was obtained by interrupting the experiments at different time intervals corresponding to the arrows indicated in **Figure 4** and analyzing by XRD the related products. The obtained results are shown in **Figure 5(a)-5(c)**. As far as the **HAp_1** is concerned, it is seen that the formation of β-TCP is evidenced at relatively low temperature (500°C), i.e. immediately after the sudden slope change manifested by the mass loss curve **(Figure 4**). Nevertheless, the corresponding sample weight loss could be mostly ascribed to the occurrence of dehydroxylation phenomena.

The XRD analysis performed when the TGA test for the **HAp_1** system was conducted at 1250°C indicated that a complete decomposition of HAp to β-TCP occurred. Minor amounts of $CaHPO_4$, originally present in the raw material, were also found at this stage. Furthermore, as the thermal analysis was prolonged to 1450°C, it is possible to observe a significant conversion of TCP from the β to the α (monoclinic) form, which represents the thermodynamically stable phase at high temperatures. This outcome is consistent with the fact that the transformation of β-TCP into the α- form is commonly reported to occur at temperatures above 1120-1170°C **[2]**.

In contrast, as evidenced in **Figure 4(b)**, no additional peaks are detected in XRD patterns of the **HAp_2** product subjected to TGA at 1250°C. This feature clearly confirms its higher thermal stability with respect to the **HAp_1** system. Therefore, the significant weight loss (about 7%) observed at 1250°C for this system (**Figure 4**) can be only associated to the dehydroxylation of HAp. Nevertheless, a completely different situation is encountered when the temperature is raised to 1450°C. Indeed, a considerable amount of TCP, particularly in its α- form, is present in the end product along with residual HAp.

A behavior qualitatively similar to that described for **HAp_2** was also displayed by the **HAp_3** material, which also exhibited a relatively high thermal stability. Specifically, as shown in **Figure 5(c)**, HAp was the only phase found by XRD in powders subjected to TGA at 1250°C. In addition, it should be noted that the amount of α- and β-TCP formed when the temperature was increased to 1450°C is even lower with respect to that found in the **HAp_2** material.

In conclusion, on the basis of the results obtained when heat treating in air the three HAp systems, **HAp_1** powders is found to display a marked thermal instability as HAp decomposes at rather low temperatures. In contrast, when the **HAp_2** and **HAp_3** powders are heat-treated in air flow, the transformation of HAp takes place only at temperatures above 1250°C to produce TCP, particularly in its α- configuration. Furthermore, the significant weight loss displayed by **HAp_1** and **HAp_2** in comparison to **HAp_3** could be likely associated to their relatively larger surface area due to the corresponding finer particles size, so that the occurrence of dehydroxylation phenomena is facilitated.

As far as the different thermal stability exhibited by the three HAp powders under examination is concerned, it should be noted that the minimum temperature to which calcium phosphate apatites decompose is well known to depend on several factors such as powders purity, particles size and shape, Ca/P molar ratio, as well as the environmental conditions under which the heat treatment is carried out [4; 22-24]. Thus, the decomposition of HAp to β-TCP taking place at relatively low temperature for the case of HAp_1 system can be readily ascribed to the presence of secondary phases ($CaHPO_4$) in the corresponding starting powders. In addition, the transformation temperature of about 750°C found in this case during heat treatment experiments in air furnace (cf. Figure 3a) is in agreement with Graeve et al. [24] findings. Specifically, in the latter study, no indication of compositional changes was evidenced by XRD after powder calcination at 600°C, whereas β-TCP **was clearly detected at 800°C. A dissociation temperature of HAp to** β-TCP **of about 700°C was also reported in the literature relatively to heat-treated calcium phosphate apatites with 1.5<Ca/P<1.667 [23]. The fact that during the TGA**

experiments conducted in the present study, β-TCP was already detected at 500°C (cf. Figure 5a) might be likely due to the air flow conditions adopted during this analysis which, apparently, are able to anticipate HAp decomposition.

Differently from the HAp_1 system, the characteristics of HAp_2 and HAp_3 powders, particularly their relatively higher purity, make them more thermally stable. In this regard, it should be noted that the temperature levels (above 1250°C) at which HAp was found to decompose to α-TCP (cf. Figures 3 and 5) are also well in agreement with the interval of 1350-1400°C reported in the literature on this subject [4; 22].

3.2 Powders consolidation by SPS

Typical outputs of sample shrinkage (δ) and temperature obtained during the densification process by SPS of HAp powders are reported in **Figure 6** for the case of the **HAp_2** system. Specifically, these data refer to the conditions of T_D=900 °C, 75 °C/min heating rate, t_D=5 min, and P=30 MPa. Only minor changes in the sample shrinkage are observed during the first 9 min of the SPS process, i.e. for temperatures below 700°C. On the other hand, as the temperature is raised above that level, the slope of the sintering curve rapidly increases approximately at a constant rate to reach a sample shrinkage of about 4 mm when the dwell temperature is achieved. Afterwards, the δ parameter modestly varies up to the end of the SPS experiment. Analogous qualitative comments can be made when examining the sintering behavior of the other systems and/or consolidation conditions investigated.

The effect of the dwell temperature on SPSed product density is shown in **Figure 7** for the different HAp materials taken into account in the present work. All the plotted data refer to sintering experiments conducted at 30 MPa, t_D=5 min and 75 °C/min heating rate. As expected, the sample densification is improved as the sintering temperature is increased, although the three processed powders displayed a quite different behavior. Indeed, while the **HAp_2** material achieved a high consolidation level at 800°C, the density values obtained by the other two materials, when processed under the same conditions, are still extremely low. In particular, the temperature condition required to produce fully dense **HAp_2** samples is 900°C, whereas the optimal temperature to achieve the same goal when starting from **HAp_3** powders is 1200°C. A peculiar behavior is observed when optimizing the sintering process for the **HAp_1** system. Specifically, a significant sample densification was evidenced in the range of 800-900°C, while a further temperature increase was accompanied only by a slight change in product density and the theoretical density value of 3.16 g/cm^3 was not achieved even at 1200°C.

The comparison of the XRD patterns of the original powders with the corresponding SPS products obtained under optimal sintering conditions is shown in **Figures 8(a)-8(c)** for the three systems.

As far as the **HAp_1** system is concerned, the first evidence of TCP formation is observed at 700°C, i.e. when the sample is less than 50% dense (**Figure 7**). Moreover, an increase of the temperature level up to 800°C is accompanied by a marked decomposition of HAp to β-TCP, which becomes the major phase in the SPS product. The amount of HAp tends to disappear when the sintering temperature is increased to 1200°C, and the corresponding material consists mainly of β-TCP. Minor amounts of $CaHPO_4$ are still detected, as in the related starting powders. Thus, the fact that the density of the SPSed product for the **HAp_1** system does not reach the theoretical value of pure HAp (**Figure 7**) can be readily ascribed to the compositional changes of the processing sample during SPS.

In contrast to the behavior described above for the **HAp_1** material and in agreement with the results obtained with the heat-treatment of raw powders, the other two systems exhibit a higher thermochemical stability during SPS. Indeed, regardless the different dwell temperatures required to obtain fully dense materials, **Figures 8(b)** and **8(c)** clearly indicate that no secondary phases are found by XRD in the fully dense **HAp_2** and **HAp_3** samples, respectively**.**

Interesting information in this regard can be also obtained when examining the gas pressure evolution inside the SPS chamber during the consolidation process. It should be noted that a vacuum pump operates continuously to maintain the pressure level in the sintering vessel at about 20 Pa. As shown in **Figure 9**, where the recorded pressure data are plotted as a function of the SPS time, a completely different behavior is exhibited by the three systems undergoing sintering. As far as the **HAp_1** and **HAp_2** powders are concerned, it is seen that after about 2.5 min, i.e. when the measured temperature was just above 200°C, the pressure value increased rapidly from the initial value to approximately 40 Pa. This fact can be associated to the beginning of dehydroxylation phenomena for both systems. However, for the case of **HAp_1**, an additional sudden increase in the pressure level was observed at about 7 min. This event began when the measured temperature was of about 500°C and can be ascribed to the initial transformation HAp→ β-TCP. Indeed, the XRD analysis relative to TGA samples (**Figure 5(a)**) evidenced the incipient presence of β-TCP at 500°C. In addition, it is important to note that when considering the **HAp_1** material, a relatively high pressure level is observed during the entire duration of the consolidation process, thus providing an indication of the progress of the hydroxyapatite decomposition. This fact is confirmed by the XRD analysis of the corresponding specimen (**Figure 8(a)**). On the other hand, during the sintering of **HAp_2** powders, the gas pressure first increases, as mentioned above, then slightly decreases and finally drops down to the initial level at about 12 min. On the basis of the XRD analysis results discussed previously, it is possible to state that the change in gas pressure for the **HAp_2** system can be only due to water losses. In addition, the fact that no gas expulsion from the sample is evidenced during the isothermal stage at 900°C, allows us to conclude that dehydroxylation phenomena correspondingly cease to occur.

In contrast to the previous finding, when the **HAp_3** powders are taken into account, the sudden pressure increase is observed only for a relatively longer sintering time, i.e. at about 12.5 min, when temperature levels above 1000°C are achieved. This outcome, which is consistent with the results obtained by TGA (**Figure 4**) as well as with the corresponding sample composition, still confirms its high thermochemical stability with respect to **HAp_1** and **HAp_2**.

Figures 10(a)-10(c) show three SEM micrographs of the sintered products obtained by SPS under optimal conditions, after being etched with a HNO_3 solution, as described in the Experimental section. First of all, it is seen that the **HAp_1** system, mostly consisting of 1-3 μm sized grains of β-TCP (**Figure 10(a)**), appears to be more sensitive, as compared to the other competitive material, to the chemical etching treatment. This feature provides an indication of the fact that HAp decomposition leads to a material which is relatively less resistant to aggressive environments. In addition, it is clear that a relatively finer microstructure, with respect to the other systems, is obtained in **HAp_2** products, as demonstrated by the corresponding sub-micrometer sized hydroxyapatite grains evidenced by the SEM micrograph shown in **Figure 10(b)**. In contrast, the sintered **HAp_3** specimen is made of relatively coarser HA grains, up to 1-3 μm in size. Such differences in the microstructure of the bulk products can be readily ascribed to the characteristics of the original powders as well as to the relatively milder sintering conditions required when processing **HAp_2** powders (**Figure 7**).

Three optical photos corresponding to optimal dense samples, about 2.4 mm thick, of the investigated HAp systems are reported in **Figures 11(a)-11(c)**. The product which displays a relatively higher transparency is **HAp_2** followed by **HAp_3,** whereas **HAp_1** appears to be the most opaque material. Such finding is consistent with the results described above. Indeed, the **HAp_2** system is obtained from the relatively more refined starting powders and no HAp decomposition was detected during the consolidation process. On the other hand, the lack of transparency in the SPSed sample obtained using **HAp_1** powders could be likely associated to the significant chemical transformations taking place during SPS (**Figure 8(a)**). Finally, although no secondary phases have been detected in the sintered **HAp_3** specimen, its relatively coarse microstructure could be responsible for the corresponding lower transparency.

3.3 Mechanical characterization

The impressions produced at 0.5 N load and 2.0 N load are exemplified in **Figure 12(a)** and **Figure 12(b)**, respectively. In particular, such micrographs were acquired on the cross section of the **HAp_2** samples, but analogous indents were induced and observed also on the other materials.

As shown in **Figure 13(a)**, the micro-hardness of the HAp sintered bodies slightly decreases when the applied load rises from 0.5 to 2.0 N, as a result of the well-known Indentation Size Effect (ISE) ~~[22]~~[25]. The local elastic modulus, instead, is less sensitive to the applied load, especially for the **HAp_1** and **HAp_2** samples, as shown in **Figure 13(b)**. Independently of the applied load, the best local mechanical properties are achieved by the **HAp_2** sintered bodies, a result that is reasonable on the basis of the mineralogical composition and compact microstructure detected for this material, as described in the previous paragraphs. The relatively low mechanical properties observed for the **HAp_1** samples with respect to the other two SPSed HAp materials are probably due to the chemical transformations occurred during sintering and the incomplete densification. However, it is worth noting that, also for the **HAp_1** samples, the hardness is well comparable to that usually reported in the literature for apatites produced with different methods. Ramesh et al. ~~[23]~~[26], for example, analyze the sintering properties of hydroxyapatite powders obtained with different methods and describe hardness values indicatively in the 50-700 HV range, whereas Curran et al. ~~[24]~~[27], comparing undoped and Sr-doped sintered HAp samples treated at 1200°C, find values in the 200-500 HV range. Also the local elastic modulus matches the values commonly observed for crystalline apatite solids (e.g. 114 GPa according to the classical study of **Gilmore et al.** ~~[25]~~[28]).

4. Summary and concluding remarks

Three commercially available HAp powders are processed in this work taking advantage of the Spark Plasma Sintering technology to rapidly obtain nearly full dense ceramics.

The starting powders differences in term of purity, particle size, microstructure, and thermo-chemical stability are found to strongly affect their sintering behavior as well as the characteristics of the resulting bulk materials. In particular, a fully dense product with no secondary phases was obtained by SPS at 900°C when using the relatively small sized, with refined grains and high purity **HAp_2** powders. On the other hand, significantly higher temperature levels (1200 °C) are required to eliminate residual porosity in the product when starting from the coarser **HAp_3** powders. Nevertheless, such temperature conditions are not so drastic to induce the formation of undesired phases in this material during its consolidation by SPS. In contrast, a marked decomposition of HAp to β-TCP, which becomes the major phase in the end product, was obtained under the same conditions (1200°C) when processing the **HAp_1** system, whose initial fine powders also contained $CaHPO_4$.

The optical, microstructural, and mechanical properties of the obtained dense bodies are consistent with the characteristics of the starting material and the corresponding SPS conditions adopted. The system exhibiting relatively higher transparency is **HAp_2** whereas the other specimens, particularly **HAp_1**, appear more opaque. This outcome is important as sample transparency enables direct viewing of living cells during biological characterization by light microscopy of the obtained materials. The achieved samples transparency can be directly associated with the related microstructures. Indeed, a **HAp_2** product consisting of sub-micrometer sized hydroxyapatite grains was obtained after the consolidation process, while relatively coarser microstructures were evidenced in the **HAp_1** and **HAp_3** end products. In addition, the transformation HAp $\rightarrow$ β-TCP occurred during sintering makes **HAp_1** more sensitive to the chemical etching with respect to the other systems where the decomposition above was avoided.

As far as the mechanical properties of the three HAp materials are concerned, it was found that they are well comparable to those ones generally reported in the literature for apatite based products fabricated via alternative methods. In particular, the best local mechanical properties are achieved by the **HAp_2** materials, whereas relatively lower hardness and elastic modulus values were obtained for the **HAp_1** samples. The good mechanical characteristics of the **HAp_2** material can be ascribed to its thermal stability and finer microstructure. On the other hand, the presence of significant amount of β-TCP in the **HAp_1** sintered product is, along with the corresponding coarser microstructure, responsible for mechanical properties worsening.

Acknowledgements

The financial support for this work from Regione Autonoma della Sardegna (Italy), L.R. n.7/2007, CUP n. F71J11001070002, is gratefully acknowledged. One of us (A.C.) has performed his activity in the framework of the PhD in Biomedical Engineering at the University of Cagliari, Italy. The authors thank Dr. Luca Desogus (University of Cagliari, Italy) for his valuable support during the experimental activity.

References

[1] Dorozhkin S.V. Bioceramics of calcium orthophosphates. Biomaterials 2010; 31(7): 1465-1485

[2] Champion E. Sintering of calcium phosphate bioceramics. Acta Biomater. 2013; 9(4): 5855-5875

[3] Bolelli G., Bellucci D., Cannillo V., Lusvarghi L., Sola A., Stiegler N., Müller P., Killinger A., Gadow R., Altomare L., De Nardo L. Suspension thermal spraying of hydroxyapatite: Microstructure and in vitro behaviour. Mat. Sci. Eng. C 2014; 34: 287-303.

[4] Cihlar J., Buchal A., Trunec M. Kinetics of thermal decomposition of hydroxyapatite bioceramics. J. Mater. Sci. 1999; 34: 6121–6131

[5] Orrù R., Licheri R., Locci A.M., Cincotti A., Cao G. Consolidation/synthesis of materials by electric current activated/assisted sintering. Mat. Sci. Eng. R 2009; 63(4-6): 127-287.

[6] Gu Y.W., Loh N.H., Khor K.A., Tor S.B., Cheang P. Spark plasma sintering of hydroxyapatite powders. Biomaterials 2002; 23(1): 37-43

[7] Nakahira A., Tamai M., Aritani H., Nakamura S., Yamashita K. Biocompatibility of dense hydroxyapatite prepared using an SPS process. J. Biomed. Mater. Res. 2002; 62(4): 550-557.

[8] Kumar R., Cheang P., Khor K.A. Spark plasma sintering and in vitro study of ultra-fine HA and ZrO_2-HA powders. J. Mater. Process. Technol. 2003; 140: 420-425

[9] Watanabe Y., Ikoma T., Monkawa A., Suetsugu Y., Yamada H., Tanaka J., Moriyoshi Y. Fabrication of transparent hydroxyapatite sintered body with high

crystal orientation by pulse electric current sintering. J. Amer. Ceram. Soc. 2005; 88(1): 243-245

[10] Guo X., Xiao P., Liu J., Shen Z. Fabrication of nanostructured hydroxyapatite via hydrothermal synthesis and spark plasma sintering. J. Amer. Ceram. Soc. 2005; 88: 1026-1029

[11] Lee B.T., Shin N.Y., Han J.K., Song H.Y. Microstructures and fracture characteristics of spark plasma-sintered HAp-5 vol.% Ag composites. Mat. Sci. Eng. A 2006; 429(1-2): 348-352

[12] Omori M., Onoki T., Hashida T., Okubo A., Murakami Y. Low temperature synthesis of hydroxyapatite from $CaHPO_4 \cdot 2H_2O$ and $Ca(OH)_2$ based on effect of the spark plasma system (SPS). Ceram. Int. 2006; 32(6): 617-621

[13] Guo X., Gough J.E., Xiao P., Liu J., Shen Z. Fabrication of nanostructured hydroxyapatite and analysis of human osteoblastic cellular response. J Biomed Mater Res A. 2007; 82(4):1022-1032.

[14] Li H., Khor K.A., Chow V., Cheang P. Nanostructural characteristics, mechanical properties, and osteoblast response of spark plasma sintered hydroxyapatite. J Biomed Mater Res A. 2007; 82(2): 296-303.

[15] Xu J.L., Khor K.A., Kumar R. Physicochemical differences after densifying radio frequency plasma sprayed hydroxyapatite powders using spark plasma and conventional sintering techniques. Mat. Sci. Eng. A 2007; 457(1-2): 24-32

[16] Gandhi A.A., Gunning R.D., Ryan K.M., Tofail S.A.M. The role of texturing and densification on optical transmittance of hydroxyapatite ceramics. J. Amer. Ceram. Soc. 2010; 93(11): 3773-3777.

[17] Eriksson M., Liu Y., Hu J., Gao L., Nygren M., Shen Z. Transparent hydroxyapatite ceramics with nanograin structure prepared by high pressure spark plasma sintering at the minimized sintering temperature. J. Eur. Ceram. Soc. 2011; 31 (9): 1533-1540

[18] Liu Y., Shen Z. Dehydroxylation of hydroxyapatite in dense bulk ceramics sintered by spark plasma sintering. J. Eur. Ceram. Soc. 2012; 32(11): 2691-2696.

[19] Kim B.N., Prajatelistia E., Han Y.H., Son H.W., Sakka Y., Kim S. Transparent hydroxyapatite ceramics consolidated by spark plasma sintering Scripta Mater. 2013; 69(5): 366-369

[20] Locci A.M., Orrù R., Cao G., Munir Z.A. Effect of ball milling on simultaneous spark plasma synthesis and densification of TiC-TiB_2 composites. Mat. Sci. Eng. A 2006; 434(1-2): 23-29.

[21] Oliver W.C., Pharr G.M. An Improved Technique for Determining Hardness and Elastic Modulus using Load and Displacement Sensing Indentation Experiments. J. Mater. Res. 1992; 7(6): 1564-1583.

[22] **Liao, C.-J., Lin, F.-H., Chen, K.-S., Sun, J.-S. Thermal decomposition and reconstitution of hydroxyapatite in air atmosphere. Biomaterials 1999; 20(19): 1807-1813.**

[23] Raynaud, S., Champion, E., Bernache-Assollant, D., Thomas, P. Calcium phosphate apatites with variable Ca/P atomic ratio I. Synthesis, characterisation and thermal stability of powders. Biomaterials 2002; 23(4): 1065-1072.

[24] Graeve, O.A., Kanakala, R., Madadi, A., Williams, B.C., Glass, K.C. Luminescence variations in hydroxyapatites doped with Eu2+ and Eu3+ ions. Biomaterials 2010; 31(15): 4259-4267

~~[22]~~[25] Milman Yu.V., Golubenko A.A., Dub S.N. Indentation size effect in nanohardness. Acta Mater. 2011; 59(20): 7480-7487.

~~[23]~~[26] Ramesh S., Aw K.L., Tolouei R., Amiriyan M., Tan C.Y., Hamdi M., Purbolaksono J., Hassan M.A., Teng W.D. Sintering properties of hydroxyapatite powders prepared using different methods. Ceram. Int. 2013; 39: 111-119.

~~[24]~~[27] Curran D.J., Fleming T.J., Towler M.R., Hampshire S. Mechanical parameters of strontium doped hydroxyapatite sintered using microwave and conventional methods. J. Mech. Behav. Biomed. Mater. 2011; 4(8): 2063-2073.

~~[25]~~[28] Gilmore R.S., Katz J.L. Elastic properties of apatites. J. Mater. Sci. 1982; 17(4): 1131-1141.

Table 1. Starting powders characteristics as provided by suppliers.

System ID	Supplier/Code	Particle size (μm)	Compositional details
HAp_1	Sigma-Aldrich Cod. 21223	25-45 (average)	≥ 90% purity (KT as $Ca_3(PO_4)_2$)
HAp_2	Alfa-Aesar Cod. 36731	< 44	Calcium phosphate tribasic, 38.1% Ca
HAp_3	Plasma Biotal Ltd Cod. CAPTAL 60-1	d_{10} = 21.7 d_{50} = 43 d_{90} = 77.8	Hydroxyapatite, Whitlockite (<1%)

Table 2. Particle size characteristics of starting powders as determined by laser light scattering analyser.

System ID	d_{10} (μm)	d_{50} (μm)	d_{90} (μm)	Average size (μm)
HAp_1	1.2	4.9	17.2	7.1
HAp_2	1.3	5.1	13.4	6.3
HAp_3	8.8	34.0	52.0	32.7

Captions for figures

Figure 1. SEM images at different magnitudes of the initial HAp powders used in the present investigation: (a)-(b) **HAp_1**, (c)-(d) **HAp_2** and (e)-(f) **HAp_3**.

Figure 2. XRD patterns on the initial HAp powders used in the present work: (a) **HAp_1**, (b) **HAp_2** and (c) **HAp_3**.

Figure 3. Effect of the heat treatment in air on the composition of (a) **HAp_1**, (b) **HAp_2** and (c) **HAp_3** powders.

Figure 4. Mass loss of HAp powders during TGA in air.

Figure 5. Compositional changes of (a) **HAp_1**, (b) **HAp_2** and (c) **HAp_3** powders during TGA (10°C/min) in air (100 ml/min).

Figure 6. Temperature and sample shrinkage time profiles recorded during consolidation of **HAp_2** powders by SPS (900°C, 75 °C/min, t_D=5 min, 30 MPa).

Figure 7. Influence of the sintering temperature on the density of the HAp products obtained by SPS (75 °C/min, t_D=5 min, 30 MPa).

Figure 8. Comparison of XRD patterns before and after consolidation by SPS (75 °C/min, t_D=5 min, 30 MPa) of (a) **HAp_1**, (b) **HAp_2** and (c) **HAp_3** powders.

Figure 9. Temporal evolution of gas pressure during the SPS process (75 °C/min, t_D=5 min, 30 MPa) of **HAp_1**, **HAp_2** and **HAp_3** powders.

Figure 10. SEM micrographs (10000 x) of chemically etched dense products obtained by SPS under optimal conditions: (a) **HAp_1**, (b) **HAp_2** and (c) **HAp_3**.

Figure 11. Optical photographs of dense products obtained by SPS under optimal conditions: (a) **HAp_1**, (b) **HAp_2** and (c) **HAp_3**.

Figure 12. Residual imprints produced in the cross section of the **HAp_2** samples during indentation tests: (a) 0.5 N and 2.0 N (b) loads.

Figure 13. Mechanical test results performed on **HAp_1**, **HAp_2** and **HAp_3** materials obtained by SPS under optimal sintering conditions: (a) micro-hardness and (b) local elastic modulus.

Figure 1. SEM images at different magnitudes of the initial HAp powders used in the present investigation: (a)-(b) **HAp_1**, (c)-(d) **HAp_2** and (e)-(f) **HAp_3**.

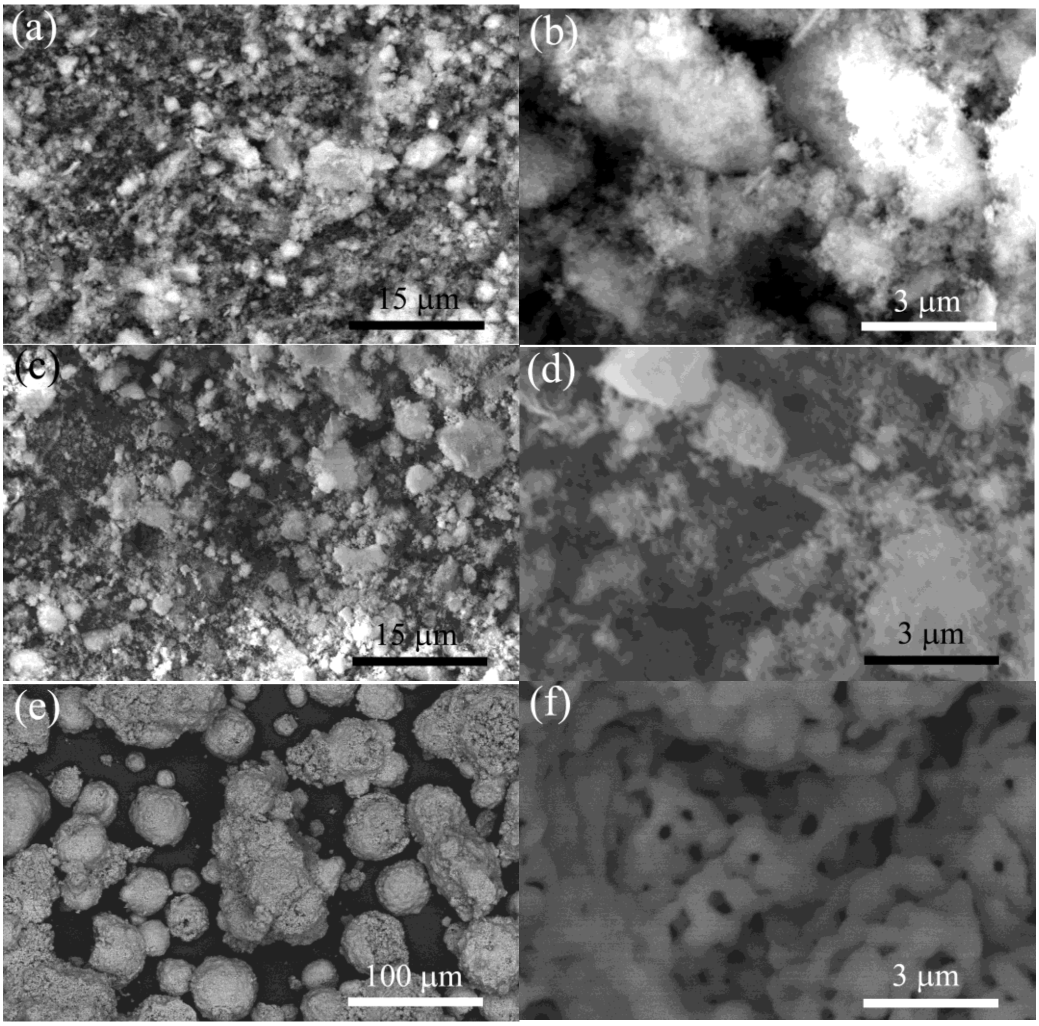

Figure 2. XRD patterns on the initial HAp powders used in the present work: (a) **HAp_1**, (b) **HAp_2** and (c) **HAp_3**.

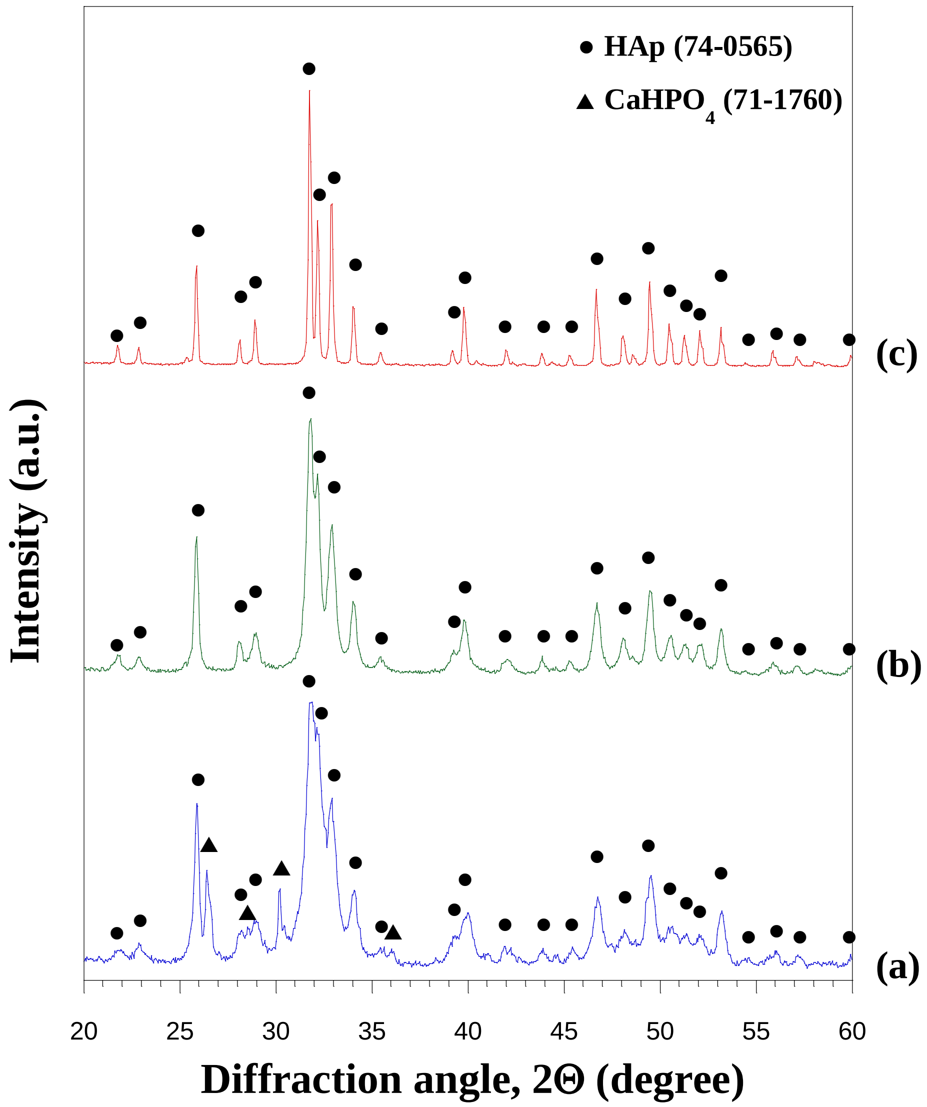

Figure 3. Effect of the heat treatment in air on the composition of (a) **HAp_1**, (b) **HAp_2** and (c) **HAp_3** powders.

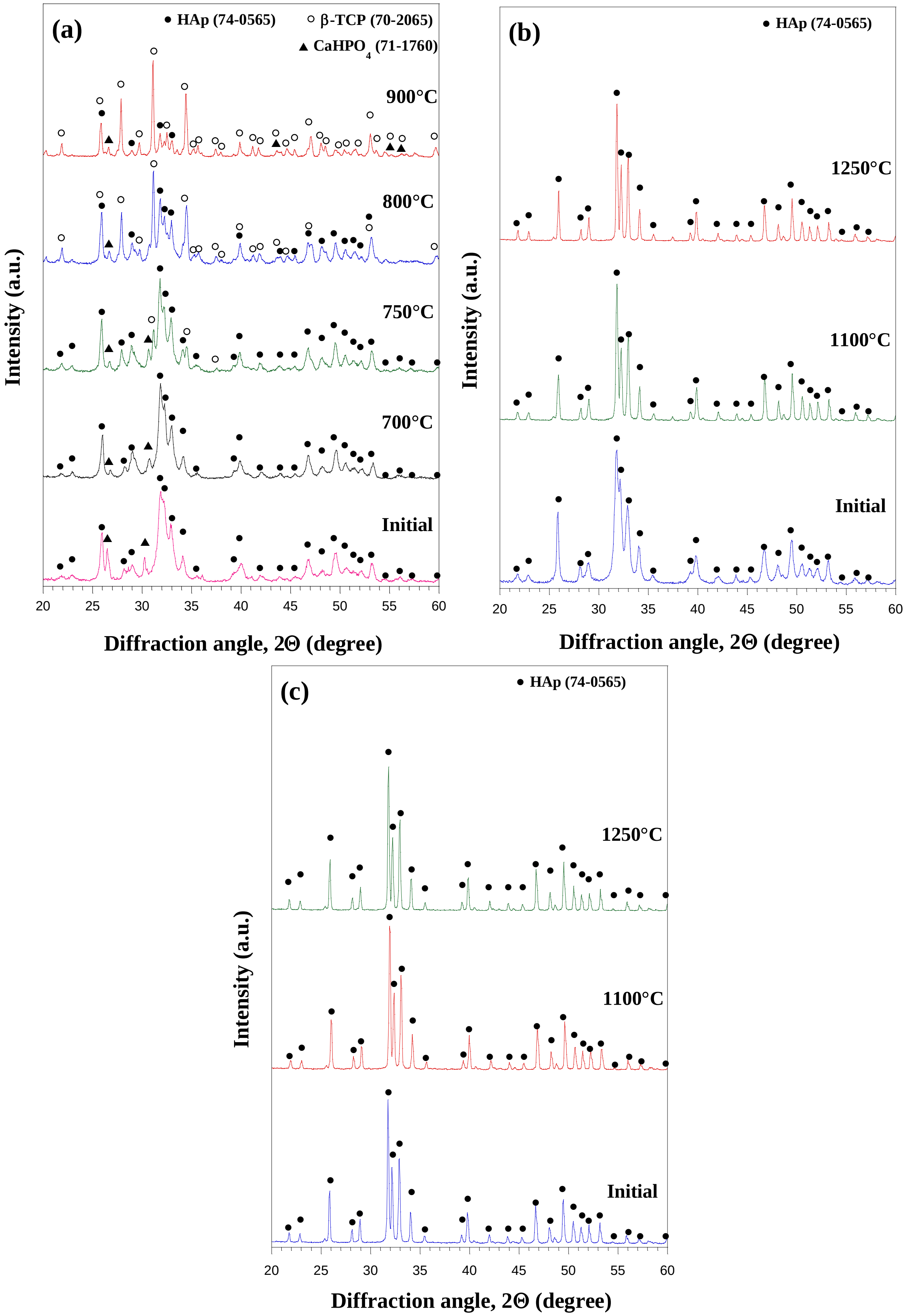

Figure 4. Mass loss of HAp powders during TGA in air.

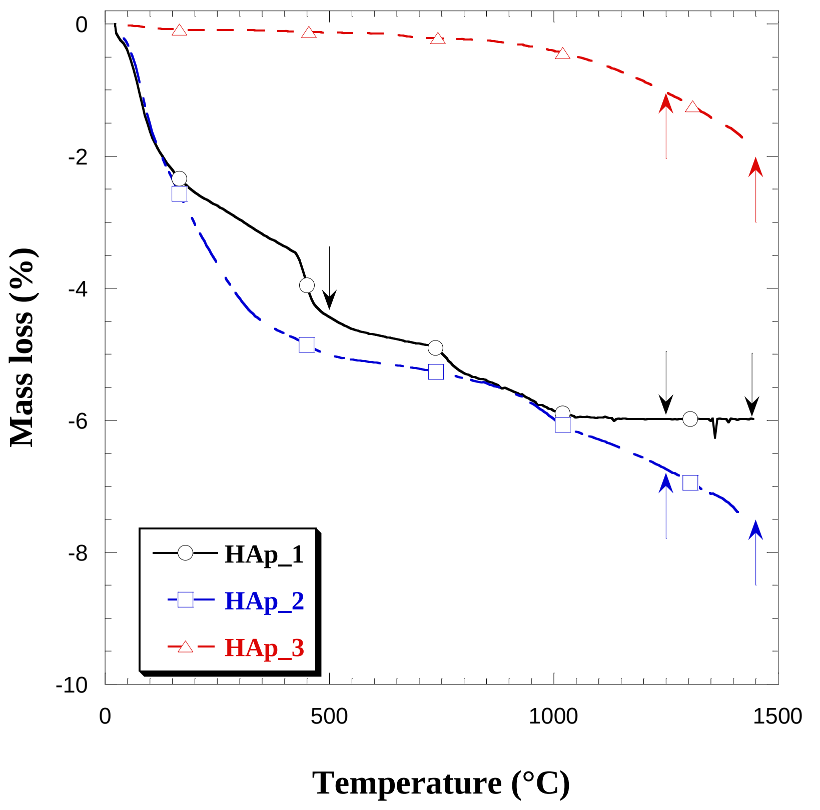

Figure 5. Compositional changes of (a) **HAp_1**, (b) **HAp_2** and (c) **HAp_3** powders during TGA (10°C/min) in air (100 ml/min) (cf. **Figure 4**).

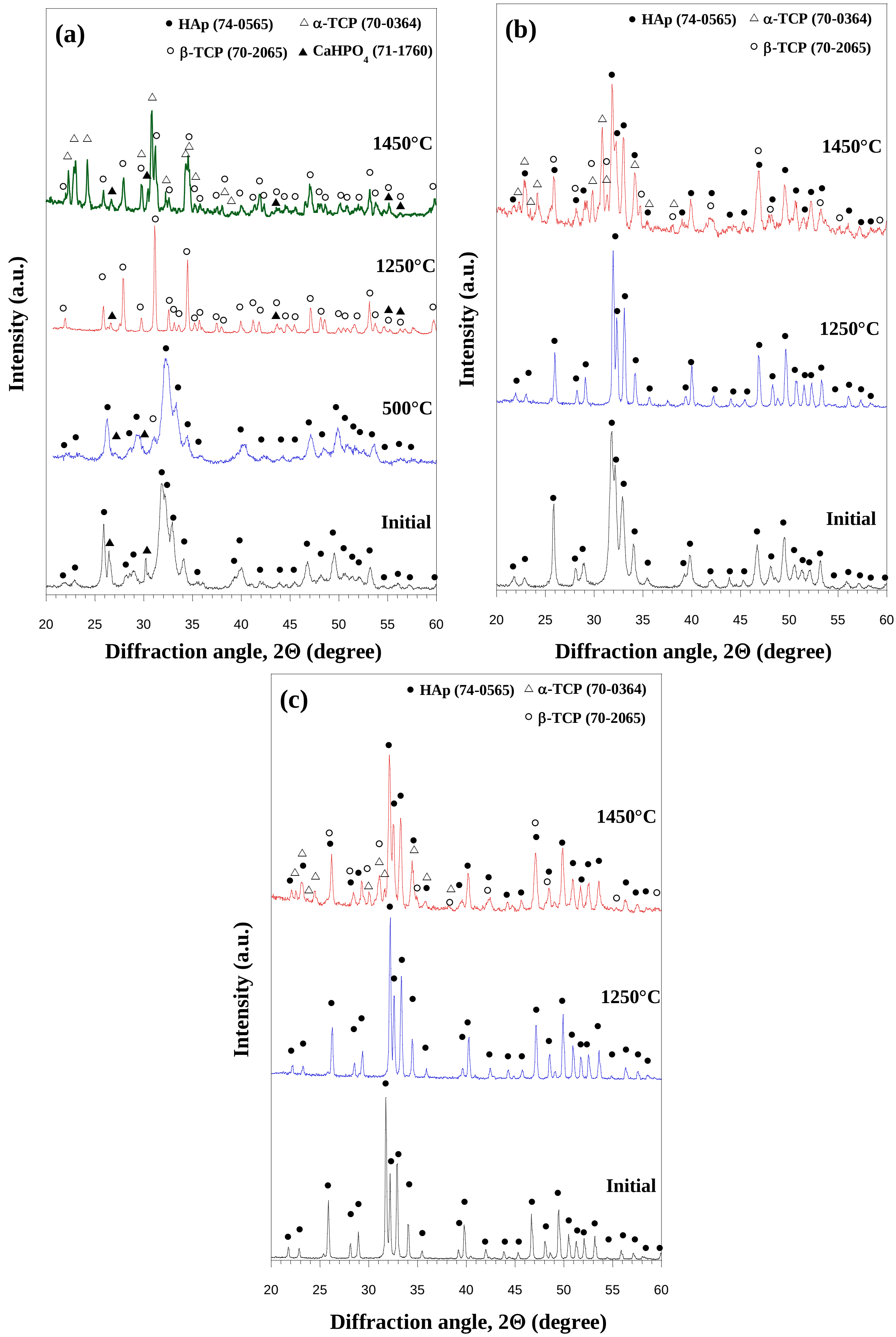

Figure 6. Temperature and sample shrinkage time profiles recorded during consolidation of **HAp_2** powders by SPS (900°C, 75 °C/min, t_D=5 min, 30 MPa).

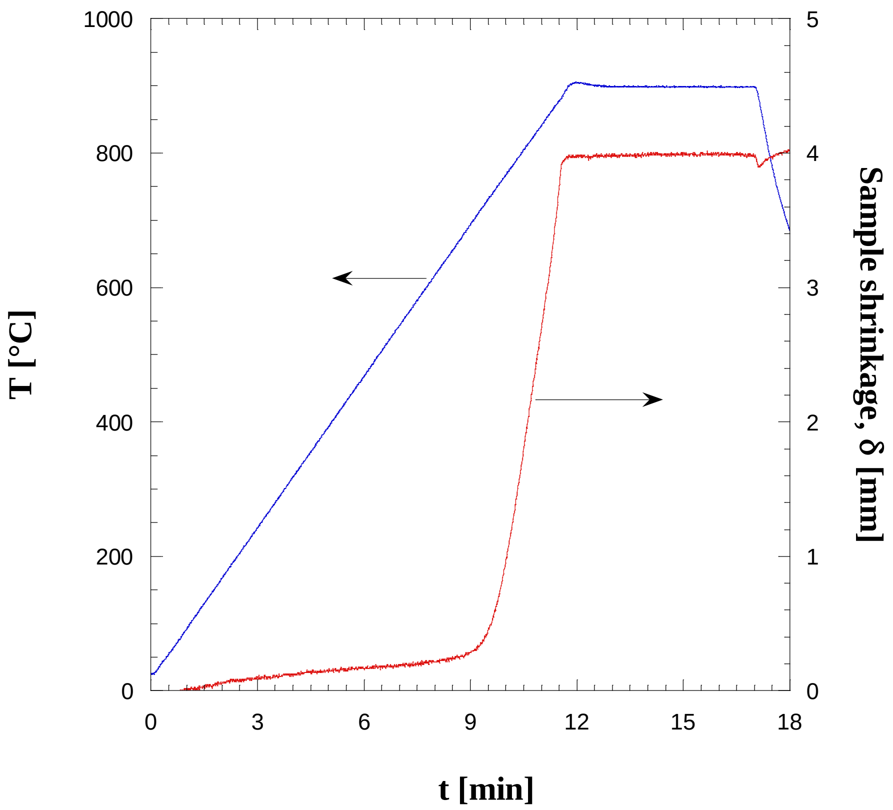

Figure 7. Influence of the sintering temperature on the density of the HAp products obtained by SPS (75 °C/min, t_D=5 min, 30 MPa).

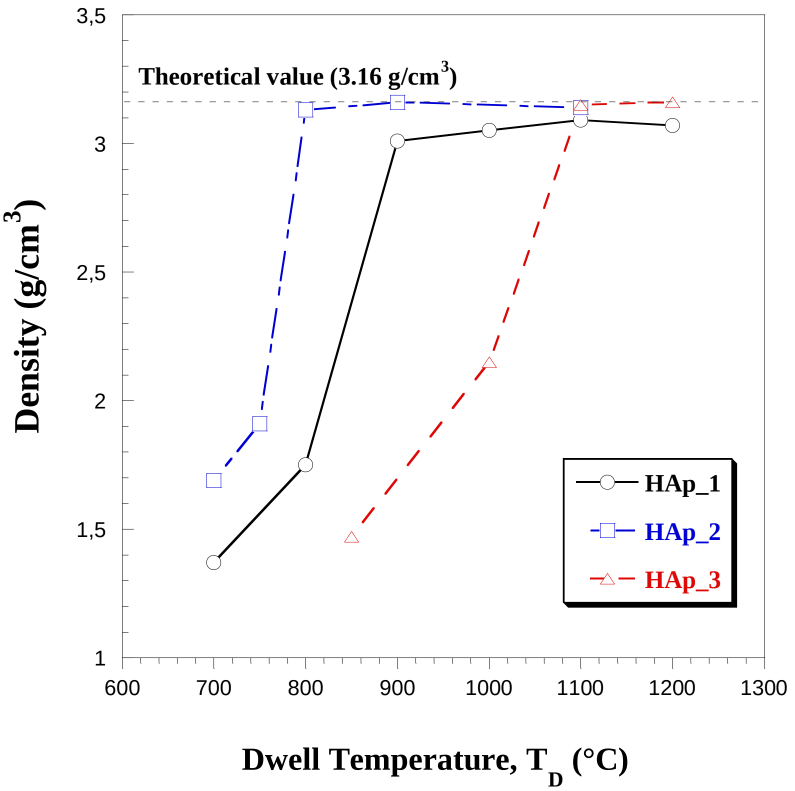

Figure 8. Comparison of XRD patterns before and after consolidation by SPS (75 °C/min, t_D=5 min, 30 MPa) of (a) **HAp_1**, (b) **HAp_2** and (c) **HAp_3** powders.

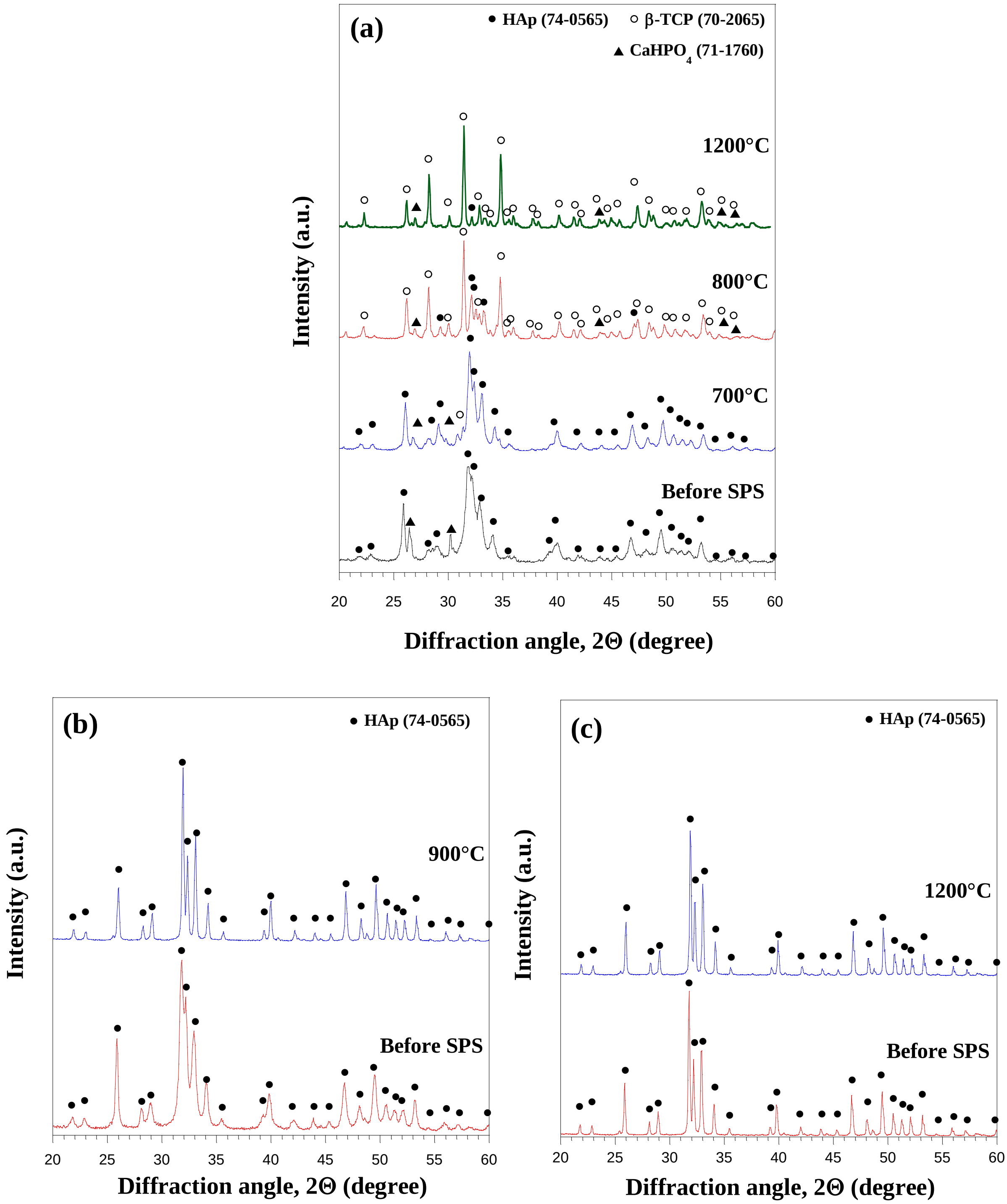

Figure 9. Temporal evolution of gas pressure during the SPS process (75 °C/min, t_D=5 min, 30 MPa) of **HAp_1**, **HAp_2** and **HAp_3** powders.

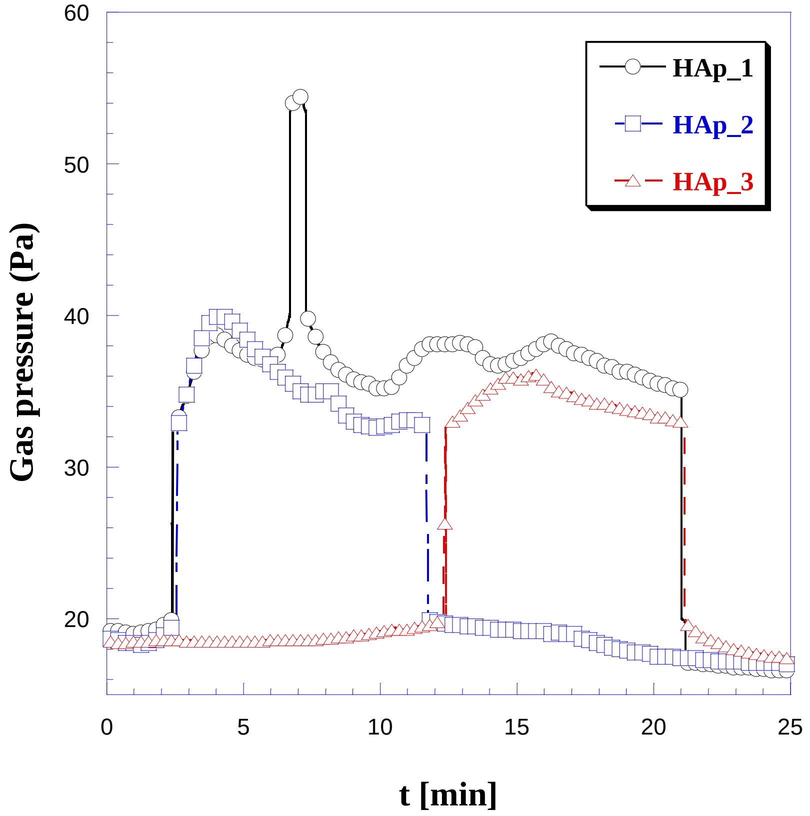

Figure 10. SEM micrographs (5000x) of chemically etched dense products obtained by SPS under optimal conditions: (a) **HAp_1**, (b) **HAp_2** and (c) **HAp_3**.

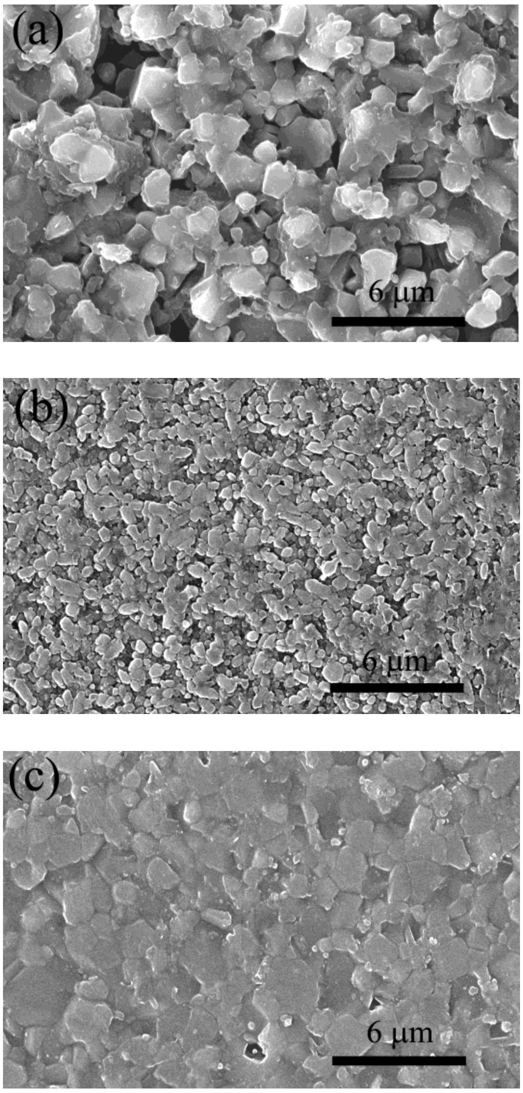

Figure 11. Optical photographs of dense products obtained by SPS under optimal conditions: (a) **HAp_1**, (b) **HAp_2** and (c) **HAp_3**.

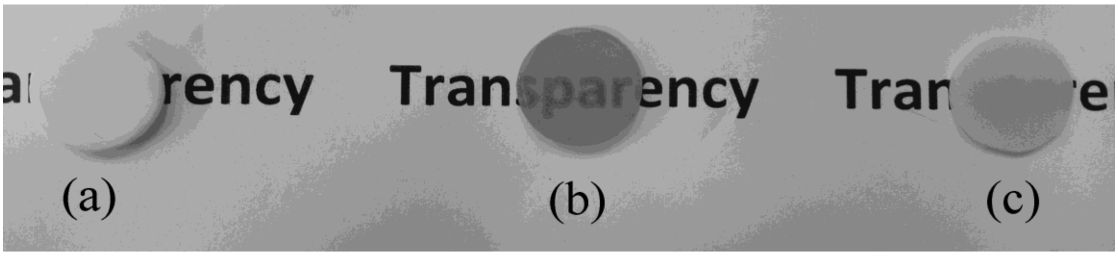

Figure 12. Residual imprints produced in the cross section of the **HAp_2** samples during indentation tests: (a) 0.5 N and 2.0 N (b) loads.

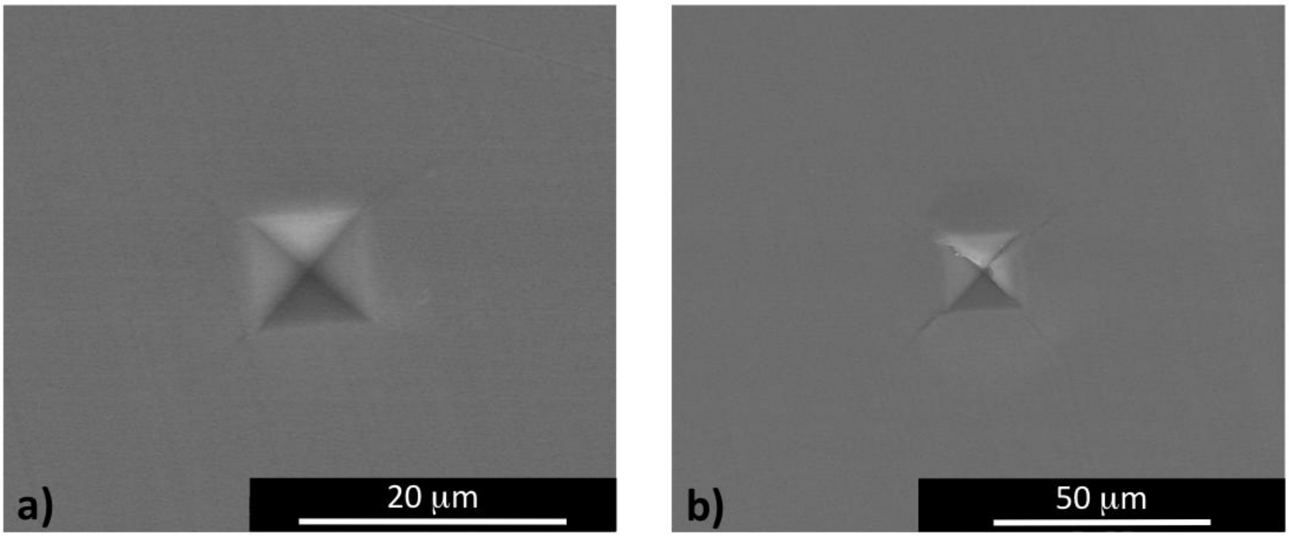

Figure 13. Mechanical test results performed on **HAp_1**, **HAp_2** and **HAp_3** materials obtained by SPS under optimal sintering conditions: (a) micro-hardness and (b) local elastic modulus.

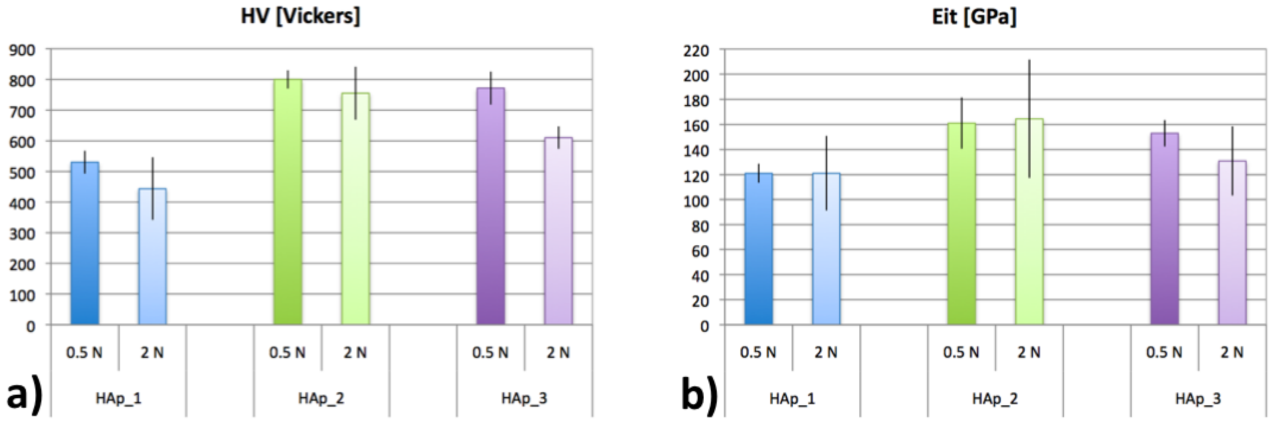

Consolidation of different Hydroxyapatite powders by SPS: optimization of the sintering conditions and characterization of the obtained bulk products

A. Cuccu[1], S. Montinaro[1], R. Orrù[1,*], G. Cao[1] , D. Bellucci[2], A. Sola[2], V. Cannillo[2]

[1]*Dipartimento di Ingegneria Meccanica, Chimica e dei Materiali, Unità di Ricerca del Consorzio Interuniversitario Nazionale per la Scienza e Tecnologia dei Materiali (INSTM) - Università degli Studi di Cagliari, via Marengo 2, 09123 Cagliari, Italy*

[2]*Dipartimento di Ingegneria "Enzo Ferrari", Università degli Studi di Modena e Reggio Emilia, Via Vignolese 905, 41125 Modena, Italy*

* Author to whom correspondence should be addressed:

R. Orrù (E-mail: roberto.orru@dimcm.unica.it; Ph.: +39-070-6755076; Fax: +39-070-6755057), *Università degli Studi di Cagliari, via Marengo 2, 09123 Cagliari, Italy*

Revised Version

August 2014

Abstract

The difference in purity, particle size, microstructure, and thermo-chemical stability of three commercially available hydroxyapatite powders are found to play an important role during their consolidation using Spark Plasma Sintering (SPS) as well as strongly affect the characteristics of the resulting sintered bodies. A fully dense material without secondary phases was obtained by SPS at 900°C, when using the relatively small sized, with refined grains and high purity powders. The sintered product, consisting of sub-micrometer sized hydroxyapatite grains, displayed optical transparency and good mechanical properties.

In contrast, the higher temperature levels (up to 1200 °C) needed to sinter powders with larger particles, or finer ones which contain additional phases, lead to products with coarser microstructures and/or significant amount of β-TCP as a result of HAp decomposition. Optical characteristics, hardness and elastic modulus of the resulting sintered samples are correspondingly worsened.

Keywords: Hydroxyapatite; Tri-Calcium Phosphate (TCP), Spark Plasma Sintering; Mechanical properties

1. Introduction

Since hydroxyapatite ($Ca_{10}(PO_4)_6(OH)_2$), often referred to as HAp or HA, represents the main inorganic component of hard human tissues (bones and teeth), it is not surprising that it is regarded as one of the most investigated ceramics for biomedical application in either bulk form or as coating **[1-3]**.

Due to its importance, a large number of research studies addressed to the fabrication of bulk HAp products using pressureless and pressure-assisted sintering methods, mainly conventional Hot Pressing (HP) or innovative Spark Plasma Sintering (SPS) techniques, have been conducted so far **[2].**

It is well known that one of the main concerns accompanying heat processing of HAp is related to its thermochemical instability **[4]**. Indeed, HAp decomposition takes place when relatively high temperature conditions are encountered during powder consolidation. Correspondingly, negative effects on mechanical and biological characteristics of the resulting materials are often produced.

In this context, the SPS technology offers a suitable method for obtaining bulk ceramic products under relatively milder sintering conditions **[5]**. Indeed, the electric pulsed current flowing directly through the die containing the non-conductive HAp powders permits sample heating at higher rates and in shorter processing times with respect to conventional HP, where external elements are employed as heating source.

Along these lines, several studies have been conducted in the literature in the last decade for the fabrication of dense HAp ceramics by SPS **[6-19]**. Most of them take advantage of the SPS technology for the consolidation of previously synthesized lab-made **[6,8-11,13-15,17,19]** or commercial **[7,10,16,18-19]** HAp powders. Alternatively, one attempt to synthesize and simultaneously densify the HAp by reactive SPS was carried out starting from $CaHPO_4 \cdot 2H_2O$ and $Ca(OH)_2$ as reaction promoters **[12]**.

As a consequence of the different starting materials, the operating conditions (i.e. holding temperature, heating rate, applied pressure and dwell time) adopted in these studies to obtain nearly full dense HAp-based bodies vary in a quite wide range, i.e. 700-1200°C. However, the potential benefits deriving from the use of SPS are confirmed. In this regard, it is clear that the characteristics of the initial powders deeply affect the final composition as well as the resulting mechanical and biological properties of the sintered material. Indeed, the decomposition of HAp to produce Tri-Calcium Phosphate (TCP) **[8,11,15]** could not be associated only to the more drastic SPS conditions correspondingly adopted. For instance, no additional phases other than HAp were found in the 99.7% dense material fabricated in 10 min by SPS at 1200°C **[9]**. On the other hand, the presence of β-TCP was evidenced by **Lee et al. [11]** in the 96.4% dense material obtained when the sintering process was conducted at 1000°C for 2 min. The use of different SPS apparatuses and sample configurations might also play a role in this regard.

In order to systematically investigate the influence of the characteristics of the initial powders on the final composition as well as the resulting mechanical properties, in the present work bulk HAp ceramics are produced by SPS using three different commercially available powders. The starting materials are first characterized by laser scattering analysis, X-ray diffraction (XRD), SEM, heat treatments in air and thermogravimetric analysis in order to highlight their main differences (purity, particle and crystallite size, thermochemical stability, etc.). Each HAp powder is then consolidated by SPS. In particular, a systematic investigation is performed to identify the optimal sintering temperatures to obtain fully dense products, while keeping all the other parameters unchanged (SPS equipment, applied pressure, heating rate, holding time, sample configuration). The resulting optimal samples are compared from the compositional, microstructural and mechanical point of view.

2. Experimental materials and methods

The main characteristics, as provided by the vendors, of the three different commercial powders investigated in this work for the fabrication of dense HAp products are reported in **Table 1**. A more detailed particle size analysis was carried out in the present study taking advantage of a laser light scattering analyser (CILAS 1180, France). The starting powders were also examined by XRD using a Philips PW 1830 X-rays diffractometer equipped with a Ni filtered Cu K_α radiation (λ=1.5405 Å). The powders' morphology was investigated by scanning electron microscopy (SEM, mod. S4000, Hitachi, Japan).

The thermal stability of the HAp powders was studied by heat treating the raw materials in air environment at different temperatures, in the range of 700-1250°C, using a laboratory furnace (Nabertherm, mod. N60/ER, Germany). In addition, a thermogravimetric analysis (TGA) under non-isothermal conditions was carried out by slowly heating (10°C/min) the initial powders from room temperature to 1450°C using a NETZSCH STA 409PC Simultaneous DTA-TGA Instrument in presence of 100 mL/min air flow.

The HAp powders were sintered in the form of cylindrical disks (about 15 mm diameter, 3 mm thickness) by Spark Plasma Sintering (SPS 515S model, Sumitomo Coal Mining Co Ltd) under vacuum conditions (20 Pa). This apparatus is based on the combination of a uniaxial press (50 kN) with a DC pulsed current generator (10 V, 1500 A, 300 Hz), thus simultaneously providing a pulsed electric current through the sample (when electrically conductive) and the graphite container, along with a mechanical pressure through the punches. The pulse cycle was set to 12 ms on and 2 ms off, being the characteristic time of single pulse equal to about 3.3 ms. Both the die and the plungers were made of AT101 graphite (Atal s.r.l., Italy). The powders to be sintered (about 1.6 g) were poured inside a cylindrical graphite die with outside diameter of 35 mm, inside diameter of 15 mm, and 30 mm high. To protect the die/plungers and make sample release easier after sintering, the compact was lined with a graphite foil (0.13 mm thick, Alfa Aesar Karlsruhe, Germany). In addition, the die was surrounded by a layer of graphite felt (3 mm thick, Atal s.r.l., Italy) for thermal insulation purpose.

The most important SPS parameters, i.e. temperature, current, voltage between the machine electrodes, mechanical load and vertical sample displacement, were recorded in real time. The displacement output provides an indication of the evolution of the powders' densification during SPS. However, the thermal expansion of sample, electrodes, graphite blocks, spacers and plungers is also responsible for the measured value. All these contributions, but that of the sample, can be separately accounted for by following a specific procedure **[20]**, thus obtaining the sample shrinkage (δ), which will be considered in what follows. In any case, the final consolidation level was determined by measuring the density of the samples obtained at the end of the SPS process. After sintering, the electric current was turned off, the mechanical load released, the sample allowed to cool to room temperature and then removed from the die. For the sake of reproducibility, each experiment was repeated at least twice.

SPS experiments were conducted under temperature controlled mode using a K-type thermocouple (Omega Engineering Inc., USA) inserted inside a small hole drilled near the center of the external surface of the graphite die. Temperature levels were also measured by means of an infrared pyrometer (CHINO, mod. IR-AHS2, Japan) focused on the lateral surface of the graphite mould.

The effect of the dwell temperature, T_D, on the product characteristics was investigated by performing all SPS experiments at constant values of the holding time (t_D=5 min), the mechanical pressure (P=30 MPa), and the heating rate (75°C/min), to achieve the desired value from the room temperature.

Relative densities were determined by the Archimedes' method after accurately polishing SPSed products and considering 3.16 g/cm^3 as theoretical value.

The microstructure of the optimal SPSed products was examined by SEM. To this aim, the sintered specimens were first mirror polished and then chemically etched for 10 s using a 3 vol.% HNO_3 solution.

The selected samples were also investigated from a mechanical point of view. A depth-sensing indentation technique was applied to determine the local elastic modulus and Vickers micro-hardness. With this aim, the samples were cut, mounted in resin and polished according to a standard metallographic procedure. The indentations were performed using an OpenPlatform instrument (CSM Instruments, Peseux, Switzerland), equipped with a Vickers indenter tip. For each sample, two different loading conditions were considered:

- low load: maximum applied load: 0.50 N; loading/unloading rate: 0.75 N/min; loading time: 15 s;
- high load: maximum applied load: 2.00 N; loading/unloading rate: 3.00 N/min; loading time: 15 s.

For statistical purposes, 30 indentations were performed for each sample and for each loading condition. For each indentation, the load-penetration depth curve was automatically acquired and then analyzed according to the Oliver and Pharr method to evaluate the local elastic properties **[21]**.

3. Results and discussion

3.1 Characterization of initial powders

The results related to the granulometry of the three different types of powders measured by laser light scattering analysis are summarized in **Table 2**. While **HAp_1** and **HAp_2** systems display similar fine particles, **HAp_3** powders are relatively coarser. This feature is clearly confirmed when examining the corresponding SEM micrographs (**Figure 1**). Specifically, both **HAp_1** and **HAp_2** materials generally consist of micrometer-sized aggregates made of sub-micrometer grains. In contrast, the **HAp_3** product exhibits coarser particles, up to 100 μm sized, characterized by a sponge like structure with pores down to 100 nm (**Figure 1(f)**).

The comparison of the corresponding XRD patterns is shown in **Figure 2**. On the basis of this analysis it is possible to state that HAp is the only phase present in **HAp_2** and **HAp_3**, while a non-negligible amount of $CaHPO_4$ was detected in **HAp_1** powders. In addition, the **HAp_1** and **HAp_2** systems displayed relatively broad diffraction peaks, to indicate their finer microstructure, in contrast to the narrow peaks observed when considering the **HAp_3** material.

The thermal stability of the starting powders was first evaluated by heat-treating the different raw materials in a furnace under air environment. The XRD spectra of the heat-treated powders are reported in **Figures 3(a)-(c)**.

No additional phases were detected by XRD when the **HAp_1** system was heat-treated at temperatures equal or lower than 700°C. On the other hand, as the temperature was raised to 750°C, the β-TCP phase (rhombohedral lattice) appeared in the XRD pattern of the end product. In addition, as higher thermal levels were achieved, the decomposition of HAp was found to increase progressively. Specifically, β-TCP becomes the major crystalline constituent in powders heat treated at 900°C, while only minor amounts of HAp and $CaHPO_4$ are present.

On the other hand, as evidenced in **Figures 3(b)** and **3(c)**, no secondary species are found in XRD patterns of **HAp_2** and **HAp_3** powders heat-treated up to 1250°C. The most significant change, particularly for **HAp_2**, is represented by a certain peak narrowing, with respect to the original material, thus indicating that grain growth is induced by the heat treatment.

In order to overcome the temperature limitation (1300°C) of the furnace utilized in the previous heat-treatment as well as to obtain further information regarding the chemico-physical stability of the powders under consideration, the latter ones have been also characterized by TGA up to 1450°C. The corresponding mass losses as a function of the temperature are plotted in **Figure 4** for the three systems. It is possible to observe that only for temperature**s** above 1000°C the **HAp_3** material significantly changes its mass. In contrast, the curves corresponding to the other two products markedly decrease just after the TGA test starts. Moreover, the weight losses resulting at the end of the experiment for **HAp_1** and **HAp_2** are 3-4 times higher than the value obtained when processing the **HAp_3** material.

The mass loss profiles described above can be associated to the compositional changes taking place in the powders as the temperature increases during the TGA test. This information was obtained by interrupting the experiments at different time intervals corresponding to the arrows indicated in **Figure 4** and analyzing by XRD the related products. The obtained results are shown in **Figure 5(a)-5(c)**. As far as the **HAp_1** is concerned, it is seen that the formation of β-TCP is evidenced at relatively low temperature (500°C), i.e. immediately after the sudden slope change manifested by the mass loss curve **(Figure 4**). Nevertheless, the corresponding sample weight loss could be mostly ascribed to the occurrence of dehydroxylation phenomena.

The XRD analysis performed when the TGA test for the **HAp_1** system was conducted at 1250°C indicated that a complete decomposition of HAp to β-TCP occurred. Minor amounts of $CaHPO_4$, originally present in the raw material, were also found at this stage. Furthermore, as the thermal analysis was prolonged to 1450°C, it is possible to observe a significant conversion of TCP from the β to the α (monoclinic) form, which represents the thermodynamically stable phase at high temperatures. This outcome is consistent with the fact that the transformation of β-TCP into the α- form is commonly reported to occur at temperatures above 1120-1170°C **[2]**.

In contrast, as evidenced in **Figure 4(b)**, no additional peaks are detected in XRD patterns of the **HAp_2** product subjected to TGA at 1250°C. This feature clearly confirms its higher thermal stability with respect to the **HAp_1** system. Therefore, the significant weight loss (about 7%) observed at 1250°C for this system (**Figure 4**) can be only associated to the dehydroxylation of HAp. Nevertheless, a completely different situation is encountered when the temperature is raised to 1450°C. Indeed, a considerable amount of TCP, particularly in its α- form, is present in the end product along with residual HAp.

A behavior qualitatively similar to that described for **HAp_2** was also displayed by the **HAp_3** material, which also exhibited a relatively high thermal stability. Specifically, as shown in **Figure 5(c)**, HAp was the only phase found by XRD in powders subjected to TGA at 1250°C. In addition, it should be noted that the amount of α- and β-TCP formed when the temperature was increased to 1450°C is even lower with respect to that found in the **HAp_2** material.

In conclusion, on the basis of the results obtained when heat treating in air the three HAp systems, **HAp_1** powders is found to display a marked thermal instability as HAp decomposes at rather low temperatures. In contrast, when the **HAp_2** and **HAp_3** powders are heat-treated in air flow, the transformation of HAp takes place only at temperatures above 1250°C to produce TCP, particularly in its α- configuration. Furthermore, the significant weight loss displayed by **HAp_1** and **HAp_2** in comparison to **HAp_3** could be likely associated to their relatively larger surface area due to the corresponding finer particles size, so that the occurrence of dehydroxylation phenomena is facilitated.

As far as the different thermal stability exhibited by the three HAp powders under examination is concerned, it should be noted that the minimum temperature to which calcium phosphate apatites decompose is well known to depend on several factors such as powders purity, particles size and shape, Ca/P molar ratio, as well as the environmental conditions under which the heat treatment is carried out **[4; 22-24]**. Thus, the decomposition of HAp to β-TCP taking place at relatively low temperature for the case of HAp_1 system can be readily ascribed to the presence of secondary phases ($CaHPO_4$) in the corresponding starting powders. In addition, the transformation temperature of about 750°C found in this case during heat treatment experiments in air furnace (cf. **Figure 3a**) is in agreement with **Graeve et al. [24]** findings. Specifically, in the latter study, no indication of compositional changes was evidenced by XRD after powder calcination at 600°C, whereas β-TCP was clearly detected at 800°C. A dissociation temperature of HAp to β-TCP of about 700°C was also reported in the literature relatively to heat-treated calcium phosphate apatites with $1.5<Ca/P<1.667$ **[23]**. The fact that during the TGA experiments conducted in the present study, β-TCP was already detected at 500°C (cf. **Figure 5a**) might be likely due to the air flow conditions adopted during this analysis which, apparently, are able to anticipate HAp decomposition.

Differently from the HAp_1 system, the characteristics of HAp_2 and HAp_3 powders, particularly their relatively higher purity, make them more thermally stable. In this regard, it should be noted that the temperature levels (above 1250°C) at which HAp was found to decompose to α-TCP (cf. **Figures 3** and **5**) are also well in agreement with the interval of 1350-1400°C reported in the literature on this subject **[4; 22]**.

3.2 Powders consolidation by SPS

Typical outputs of sample shrinkage (δ) and temperature obtained during the densification process by SPS of HAp powders are reported in **Figure 6** for the case of the **HAp_2** system. Specifically, these data refer to the conditions of T_D=900 °C, 75 °C/min heating rate, t_D=5 min, and P=30 MPa. Only minor changes in the sample shrinkage are observed during the first 9 min of the SPS process, i.e. for temperatures below 700°C. On the other hand, as the temperature is raised above that level, the slope of the sintering curve rapidly increases approximately at a constant rate to reach a sample shrinkage of about 4 mm when the dwell temperature is achieved. Afterwards, the δ parameter modestly varies up to the end of the SPS experiment. Analogous qualitative comments can be made when examining the sintering behavior of the other systems and/or consolidation conditions investigated.

The effect of the dwell temperature on SPSed product density is shown in **Figure 7** for the different HAp materials taken into account in the present work. All the plotted data refer to sintering experiments conducted at 30 MPa, t_D=5 min and 75

°C/min heating rate. As expected, the sample densification is improved as the sintering temperature is increased, although the three processed powders displayed a quite different behavior. Indeed, while the **HAp_2** material achieved a high consolidation level at 800°C, the density values obtained by the other two materials, when processed under the same conditions, are still extremely low. In particular, the temperature condition required to produce fully dense **HAp_2** samples is 900°C, whereas the optimal temperature to achieve the same goal when starting from **HAp_3** powders is 1200°C. A peculiar behavior is observed when optimizing the sintering process for the **HAp_1** system. Specifically, a significant sample densification was evidenced in the range of 800-900°C, while a further temperature increase was accompanied only by a slight change in product density and the theoretical density value of 3.16 g/cm^3 was not achieved even at 1200°C.

The comparison of the XRD patterns of the original powders with the corresponding SPS products obtained under optimal sintering conditions is shown in **Figures 8(a)-8(c)** for the three systems.

As far as the **HAp_1** system is concerned, the first evidence of TCP formation is observed at 700°C, i.e. when the sample is less than 50% dense (**Figure 7**). Moreover, an increase of the temperature level up to 800°C is accompanied by a marked decomposition of HAp to β-TCP, which becomes the major phase in the SPS product. The amount of HAp tends to disappear when the sintering temperature is increased to 1200°C, and the corresponding material consists mainly of β-TCP. Minor amounts of $CaHPO_4$ are still detected, as in the related starting powders. Thus, the fact that the density of the SPSed product for the **HAp_1** system does not reach the theoretical value of pure HAp (**Figure 7**) can be readily ascribed to the compositional changes of the processing sample during SPS.

In contrast to the behavior described above for the **HAp_1** material and in agreement with the results obtained with the heat-treatment of raw powders, the other two systems exhibit a higher thermochemical stability during SPS. Indeed, regardless the different dwell temperatures required to obtain fully dense materials, **Figures 8(b)** and **8(c)** clearly indicate that no secondary phases are found by XRD in the fully dense **HAp_2** and **HAp_3** samples, respectively**.**

Interesting information in this regard can be also obtained when examining the gas pressure evolution inside the SPS chamber during the consolidation process. It should be noted that a vacuum pump operates continuously to maintain the pressure level in the sintering vessel at about 20 Pa. As shown in **Figure 9**, where the recorded pressure data are plotted as a function of the SPS time, a completely different behavior is exhibited by the three systems undergoing sintering. As far as the **HAp_1** and **HAp_2** powders are concerned, it is seen that after about 2.5 min, i.e. when the measured temperature was just above 200°C, the pressure value increased rapidly from the initial value to approximately 40 Pa. This fact can be associated to the beginning of dehydroxylation phenomena for both systems. However, for the case of **HAp_1**, an additional sudden increase in the pressure level was observed at about 7 min. This event began when the measured temperature was of about 500°C and can be ascribed to the initial transformation HAp→ β-TCP. Indeed, the XRD analysis relative to TGA samples (**Figure 5(a)**) evidenced the incipient presence of β-TCP at 500°C. In addition, it is important to note that when considering the **HAp_1** material, a relatively high pressure level is observed during the entire duration of the consolidation process, thus providing an indication of the progress of the hydroxyapatite decomposition. This fact is confirmed by the XRD analysis of the corresponding specimen (**Figure 8(a)**). On the other hand, during the sintering of **HAp_2** powders, the gas pressure first increases, as mentioned above, then slightly decreases and finally drops down to the initial level at about 12 min. On the basis of the XRD analysis results discussed previously, it is possible to state that the change in gas pressure for the **HAp_2** system can be only due to water losses. In addition, the fact that no gas expulsion from the sample is evidenced during the isothermal stage at 900°C, allows us to conclude that dehydroxylation phenomena correspondingly cease to occur.

In contrast to the previous finding, when the **HAp_3** powders are taken into account, the sudden pressure increase is observed only for a relatively longer sintering time, i.e. at about 12.5 min, when temperature levels above 1000°C are achieved. This outcome, which is consistent with the results obtained by TGA (**Figure 4**) as well as with the corresponding sample composition, still confirms its high thermochemical stability with respect to **HAp_1** and **HAp_2**.

Figures 10(a)-10(c) show three SEM micrographs of the sintered products obtained by SPS under optimal conditions, after being etched with a HNO_3 solution, as described in the Experimental section. First of all, it is seen that the **HAp_1** system, mostly consisting of 1-3 μm sized grains of β-TCP (**Figure 10(a)**), appears to be more sensitive, as compared to the other competitive material, to the chemical etching treatment. This feature provides an indication of the fact that HAp decomposition leads to a material which is relatively less resistant to aggressive environments. In addition, it is clear that a relatively finer microstructure, with respect to the other systems, is obtained in **HAp_2** products, as demonstrated by the corresponding sub-micrometer sized hydroxyapatite grains evidenced by the SEM micrograph shown in **Figure 10(b)**. In contrast, the sintered **HAp_3** specimen is made of relatively coarser HA grains, up to 1-3 μm in size. Such differences in the microstructure of the bulk products can be readily ascribed to the characteristics of the original powders as well as to the relatively milder sintering conditions required when processing **HAp_2** powders (**Figure 7**).

Three optical photos corresponding to optimal dense samples, about 2.4 mm thick, of the investigated HAp systems are reported in **Figures 11(a)-11(c)**. The product which displays a relatively higher transparency is **HAp_2** followed by **HAp_3,** whereas **HAp_1** appears to be the most opaque material. Such finding is consistent with the results described above. Indeed, the **HAp_2** system is obtained from the relatively more refined starting powders and no HAp decomposition was detected during the consolidation process. On the other hand, the lack of transparency in the SPSed sample obtained using **HAp_1** powders could be likely associated to the significant chemical transformations taking place during SPS (**Figure 8(a)**). Finally, although no secondary phases have been detected in the sintered **HAp_3** specimen, its relatively coarse microstructure could be responsible for the corresponding lower transparency.

3.3 Mechanical characterization

The impressions produced at 0.5 N load and 2.0 N load are exemplified in **Figure 12(a)** and **Figure 12(b)**, respectively. In particular, such micrographs were acquired on the cross section of the **HAp_2** samples, but analogous indents were induced and observed also on the other materials.

As shown in **Figure 13(a)**, the micro-hardness of the HAp sintered bodies slightly decreases when the applied load rises from 0.5 to 2.0 N, as a result of the well-known Indentation Size Effect (ISE) **[25]**. The local elastic modulus, instead, is less sensitive to the applied load, especially for the **HAp_1** and **HAp_2** samples, as shown in **Figure 13(b)**. Independently of the applied load, the best local mechanical properties are achieved by the **HAp_2** sintered bodies, a result that is reasonable on the basis of the mineralogical composition and compact microstructure detected for this material, as described in the previous paragraphs. The relatively low mechanical properties observed for the **HAp_1** samples with respect to the other two SPSed HAp materials are probably due to the chemical transformations occurred during sintering and the incomplete densification. However, it is worth noting that, also for the **HAp_1** samples, the hardness is well comparable to that usually reported in the literature for apatites produced with different methods. **Ramesh et al. [26]**, for example, analyze the sintering properties of hydroxyapatite powders obtained with different methods and describe hardness values indicatively in the 50-700 HV range, whereas **Curran et al. [27]**, comparing undoped and Sr-doped sintered HAp samples treated at 1200°C, find values in the 200-500 HV range. Also the local elastic modulus matches the values commonly observed for crystalline apatite solids (e.g. 114 GPa according to the classical study of **Gilmore et al. [28]**).

4. Summary and concluding remarks

Three commercially available HAp powders are processed in this work taking advantage of the Spark Plasma Sintering technology to rapidly obtain nearly full dense ceramics.

The starting powders differences in term of purity, particle size, microstructure, and thermo-chemical stability are found to strongly affect their sintering behavior as well as the characteristics of the resulting bulk materials. In particular, a fully dense product with no secondary phases was obtained by SPS at 900°C when using the relatively small sized, with refined grains and high purity **HAp_2** powders. On the other hand, significantly higher temperature levels (1200 °C) are required to eliminate residual porosity in the product when starting from the coarser **HAp_3** powders. Nevertheless, such temperature conditions are not so drastic to induce the formation of undesired phases in this material during its consolidation by SPS. In contrast, a marked decomposition of HAp to β-TCP, which becomes the major phase in the end product, was obtained under the same conditions (1200°C) when processing the **HAp_1** system, whose initial fine powders also contained $CaHPO_4$.

The optical, microstructural, and mechanical properties of the obtained dense bodies are consistent with the characteristics of the starting material and the corresponding SPS conditions adopted. The system exhibiting relatively higher transparency is **HAp_2** whereas the other specimens, particularly **HAp_1**, appear more opaque. This outcome is important as sample transparency enables direct viewing of living cells during biological characterization by light microscopy of the obtained materials. The achieved samples transparency can be directly associated with the related microstructures. Indeed, a **HAp_2** product consisting of sub-micrometer sized hydroxyapatite grains was obtained after the consolidation process, while relatively coarser microstructures were evidenced in the **HAp_1** and **HAp_3** end products. In addition, the transformation HAp → β-TCP occurred during sintering makes **HAp_1** more sensitive to the chemical etching with respect to the other systems where the decomposition above was avoided.

As far as the mechanical properties of the three HAp materials are concerned, it was found that they are well comparable to those ones generally reported in the literature for apatite based products fabricated via alternative methods. In particular, the best local mechanical properties are achieved by the **HAp_2** materials, whereas relatively lower hardness and elastic modulus values were obtained for the **HAp_1** samples. The good mechanical characteristics of the **HAp_2** material can be ascribed to its thermal stability and finer microstructure. On the other hand, the presence of significant amount of β-TCP in the **HAp_1** sintered product is, along with the corresponding coarser microstructure, responsible for mechanical properties worsening.

Acknowledgements

The financial support for this work from Regione Autonoma della Sardegna (Italy), L.R. n.7/2007, CUP n. F71J11001070002, is gratefully acknowledged. One of us (A.C.) has performed his activity in the framework of the PhD in Biomedical Engineering at the University of Cagliari, Italy. The authors thank Dr. Luca Desogus (University of Cagliari, Italy) for his valuable support during the experimental activity.

References

[1] Dorozhkin S.V. Bioceramics of calcium orthophosphates. Biomaterials 2010; 31(7): 1465-1485

[2] Champion E. Sintering of calcium phosphate bioceramics. Acta Biomater. 2013; 9(4): 5855-5875

[3] Bolelli G., Bellucci D., Cannillo V., Lusvarghi L., Sola A., Stiegler N., Müller P., Killinger A., Gadow R., Altomare L., De Nardo L. Suspension thermal spraying of hydroxyapatite: Microstructure and in vitro behaviour. Mat. Sci. Eng. C 2014; 34: 287-303.

[4] Cihlar J., Buchal A., Trunec M. Kinetics of thermal decomposition of hydroxyapatite bioceramics. J. Mater. Sci. 1999; 34: 6121–6131

[5] Orrù R., Licheri R., Locci A.M., Cincotti A., Cao G. Consolidation/synthesis of materials by electric current activated/assisted sintering. Mat. Sci. Eng. R 2009; 63(4-6): 127-287.

[6] Gu Y.W., Loh N.H., Khor K.A., Tor S.B., Cheang P. Spark plasma sintering of hydroxyapatite powders. Biomaterials 2002; 23(1): 37-43

[7] Nakahira A., Tamai M., Aritani H., Nakamura S., Yamashita K. Biocompatibility of dense hydroxyapatite prepared using an SPS process. J. Biomed. Mater. Res. 2002; 62(4): 550-557.

[8] Kumar R., Cheang P., Khor K.A. Spark plasma sintering and in vitro study of ultra-fine HA and ZrO_2-HA powders. J. Mater. Process. Technol. 2003; 140: 420-425

[9] Watanabe Y., Ikoma T., Monkawa A., Suetsugu Y., Yamada H., Tanaka J., Moriyoshi Y. Fabrication of transparent hydroxyapatite sintered body with high

crystal orientation by pulse electric current sintering. J. Amer. Ceram. Soc. 2005; 88(1): 243-245

[10] Guo X., Xiao P., Liu J., Shen Z. Fabrication of nanostructured hydroxyapatite via hydrothermal synthesis and spark plasma sintering. J. Amer. Ceram. Soc. 2005; 88: 1026-1029

[11] Lee B.T., Shin N.Y., Han J.K., Song H.Y. Microstructures and fracture characteristics of spark plasma-sintered HAp-5 vol.% Ag composites. Mat. Sci. Eng. A 2006; 429(1-2): 348-352

[12] Omori M., Onoki T., Hashida T., Okubo A., Murakami Y. Low temperature synthesis of hydroxyapatite from $CaHPO_4{\cdot}2H_2O$ and $Ca(OH)_2$ based on effect of the spark plasma system (SPS). Ceram. Int. 2006; 32(6): 617-621

[13] Guo X., Gough J.E., Xiao P., Liu J., Shen Z. Fabrication of nanostructured hydroxyapatite and analysis of human osteoblastic cellular response. J Biomed Mater Res A. 2007; 82(4):1022-1032.

[14] Li H., Khor K.A., Chow V., Cheang P. Nanostructural characteristics, mechanical properties, and osteoblast response of spark plasma sintered hydroxyapatite. J Biomed Mater Res A. 2007; 82(2): 296-303.

[15] Xu J.L., Khor K.A., Kumar R. Physicochemical differences after densifying radio frequency plasma sprayed hydroxyapatite powders using spark plasma and conventional sintering techniques. Mat. Sci. Eng. A 2007; 457(1-2): 24-32

[16] Gandhi A.A., Gunning R.D., Ryan K.M., Tofail S.A.M. The role of texturing and densification on optical transmittance of hydroxyapatite ceramics. J. Amer. Ceram. Soc. 2010; 93(11): 3773-3777.

[17] Eriksson M., Liu Y., Hu J., Gao L., Nygren M., Shen Z. Transparent hydroxyapatite ceramics with nanograin structure prepared by high pressure spark plasma sintering at the minimized sintering temperature. J. Eur. Ceram. Soc. 2011; 31 (9): 1533-1540

[18] Liu Y., Shen Z. Dehydroxylation of hydroxyapatite in dense bulk ceramics sintered by spark plasma sintering. J. Eur. Ceram. Soc. 2012; 32(11): 2691-2696.

[19] Kim B.N., Prajatelistia E., Han Y.H., Son H.W., Sakka Y., Kim S. Transparent hydroxyapatite ceramics consolidated by spark plasma sintering Scripta Mater. 2013; 69(5): 366-369

[20] Locci A.M., Orrù R., Cao G., Munir Z.A. Effect of ball milling on simultaneous spark plasma synthesis and densification of TiC-TiB_2 composites. Mat. Sci. Eng. A 2006; 434(1-2): 23-29.

[21] Oliver W.C., Pharr G.M. An Improved Technique for Determining Hardness and Elastic Modulus using Load and Displacement Sensing Indentation Experiments. J. Mater. Res. 1992; 7(6): 1564-1583.

[22] Liao, C.-J., Lin, F.-H., Chen, K.-S., Sun, J.-S. Thermal decomposition and reconstitution of hydroxyapatite in air atmosphere. Biomaterials 1999; 20(19): 1807-1813.

[23] Raynaud, S., Champion, E., Bernache-Assollant, D., Thomas, P. Calcium phosphate apatites with variable Ca/P atomic ratio I. Synthesis, characterisation and thermal stability of powders. Biomaterials 2002; 23(4): 1065-1072.

[24] Graeve, O.A., Kanakala, R., Madadi, A., Williams, B.C., Glass, K.C. Luminescence variations in hydroxyapatites doped with Eu2+ and Eu3+ ions. Biomaterials 2010; 31(15): 4259-4267

[25] Milman Yu.V., Golubenko A.A., Dub S.N. Indentation size effect in nanohardness. Acta Mater. 2011; 59(20): 7480-7487.

[26] Ramesh S., Aw K.L., Tolouei R., Amiriyan M., Tan C.Y., Hamdi M., Purbolaksono J., Hassan M.A., Teng W.D. Sintering properties of hydroxyapatite powders prepared using different methods. Ceram. Int. 2013; 39: 111-119.

[27] Curran D.J., Fleming T.J., Towler M.R., Hampshire S. Mechanical parameters of strontium doped hydroxyapatite sintered using microwave and conventional methods. J. Mech. Behav. Biomed. Mater. 2011; 4(8): 2063-2073.

[28] Gilmore R.S., Katz J.L. Elastic properties of apatites. J. Mater. Sci. 1982; 17(4): 1131-1141.

Table 1. Starting powders characteristics as provided by suppliers.

System ID	Supplier/Code	Particle size (μm)	Compositional details
HAp_1	Sigma-Aldrich Cod. 21223	25-45 (average)	≥ 90% purity (KT as $Ca_3(PO_4)_2$)
HAp_2	Alfa-Aesar Cod. 36731	< 44	Calcium phosphate tribasic, 38.1% Ca
HAp_3	Plasma Biotal Ltd Cod. CAPTAL 60-1	d_{10} = 21.7 d_{50} = 43 d_{90} = 77.8	Hydroxyapatite, Whitlockite (<1%)

Table 2. Particle size characteristics of starting powders as determined by laser light scattering analyser.

System ID	d_{10} (μm)	d_{50} (μm)	d_{90} (μm)	Average size (μm)
HAp_1	1.2	4.9	17.2	7.1
HAp_2	1.3	5.1	13.4	6.3
HAp_3	8.8	34.0	52.0	32.7

Captions for figures

Figure 1. SEM images at different magnitudes of the initial HAp powders used in the present investigation: (a)-(b) **HAp_1**, (c)-(d) **HAp_2** and (e)-(f) **HAp_3**.

Figure 2. XRD patterns on the initial HAp powders used in the present work: (a) **HAp_1**, (b) **HAp_2** and (c) **HAp_3**.

Figure 3. Effect of the heat treatment in air on the composition of (a) **HAp_1**, (b) **HAp_2** and (c) **HAp_3** powders.

Figure 4. Mass loss of HAp powders during TGA in air.

Figure 5. Compositional changes of (a) **HAp_1**, (b) **HAp_2** and (c) **HAp_3** powders during TGA (10°C/min) in air (100 ml/min).

Figure 6. Temperature and sample shrinkage time profiles recorded during consolidation of **HAp_2** powders by SPS (900°C, 75 °C/min, t_D=5 min, 30 MPa).

Figure 7. Influence of the sintering temperature on the density of the HAp products obtained by SPS (75 °C/min, t_D=5 min, 30 MPa).

Figure 8. Comparison of XRD patterns before and after consolidation by SPS (75 °C/min, t_D=5 min, 30 MPa) of (a) **HAp_1**, (b) **HAp_2** and (c) **HAp_3** powders.

Figure 9. Temporal evolution of gas pressure during the SPS process (75 °C/min, t_D=5 min, 30 MPa) of **HAp_1**, **HAp_2** and **HAp_3** powders.

Figure 10. SEM micrographs (10000 x) of chemically etched dense products obtained by SPS under optimal conditions: (a) **HAp_1**, (b) **HAp_2** and (c) **HAp_3**.

Figure 11. Optical photographs of dense products obtained by SPS under optimal conditions: (a) **HAp_1**, (b) **HAp_2** and (c) **HAp_3**.

Figure 12. Residual imprints produced in the cross section of the **HAp_2** samples during indentation tests: (a) 0.5 N and 2.0 N (b) loads.

Figure 13. Mechanical test results performed on **HAp_1**, **HAp_2** and **HAp_3** materials obtained by SPS under optimal sintering conditions: (a) micro-hardness and (b) local elastic modulus.

Figure 1. SEM images at different magnitudes of the initial HAp powders used in the present investigation: (a)-(b) **HAp_1**, (c)-(d) **HAp_2** and (e)-(f) **HAp_3**.

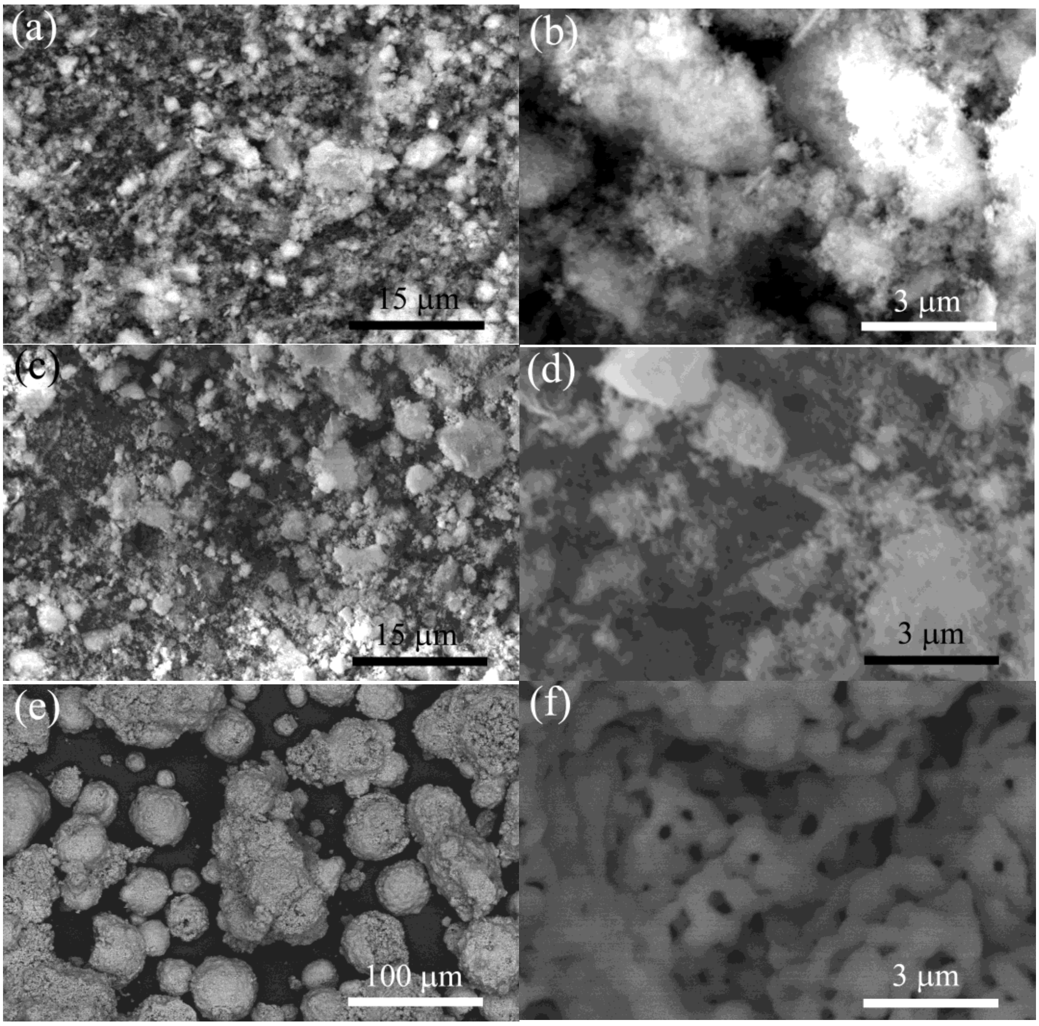

Figure 2. XRD patterns on the initial HAp powders used in the present work: (a) **HAp_1**, (b) **HAp_2** and (c) **HAp_3**.

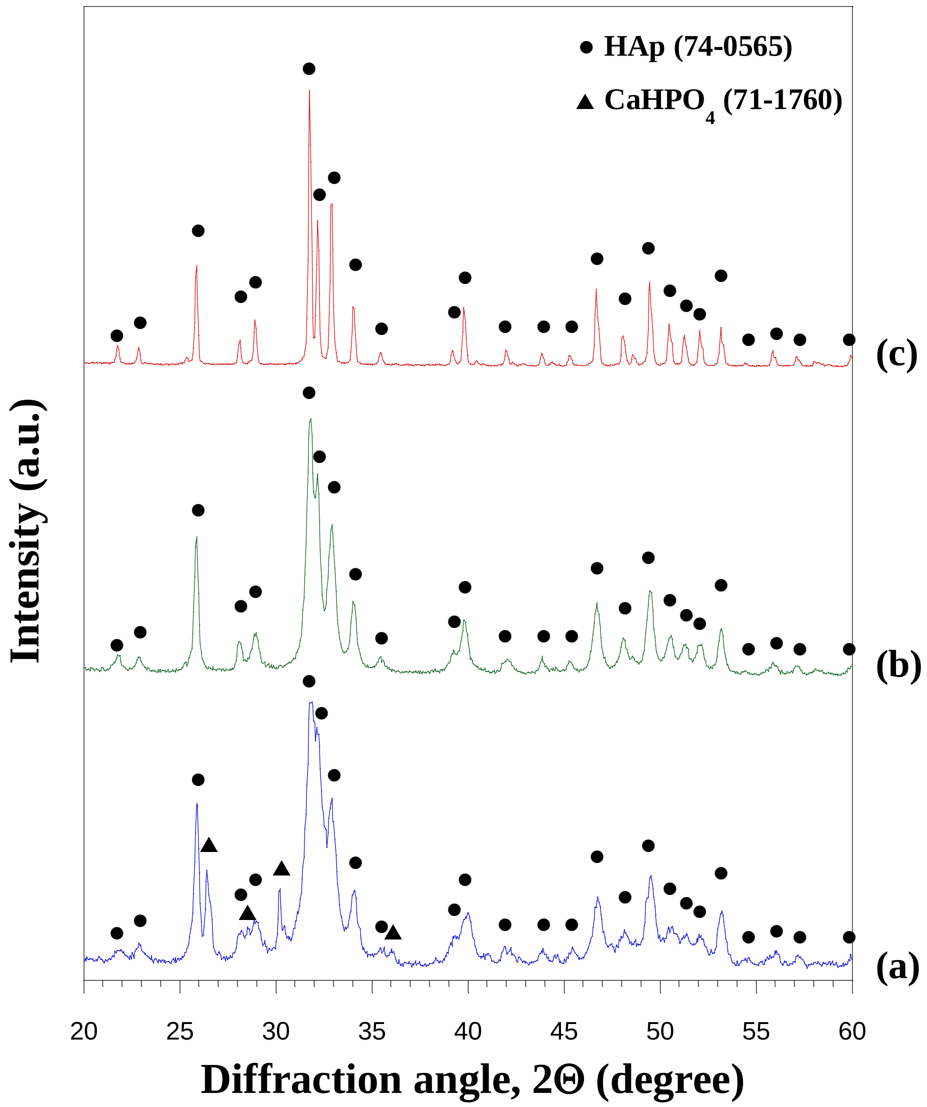

Figure 3. Effect of the heat treatment in air on the composition of (a) **HAp_1**, (b) **HAp_2** and (c) **HAp_3** powders.

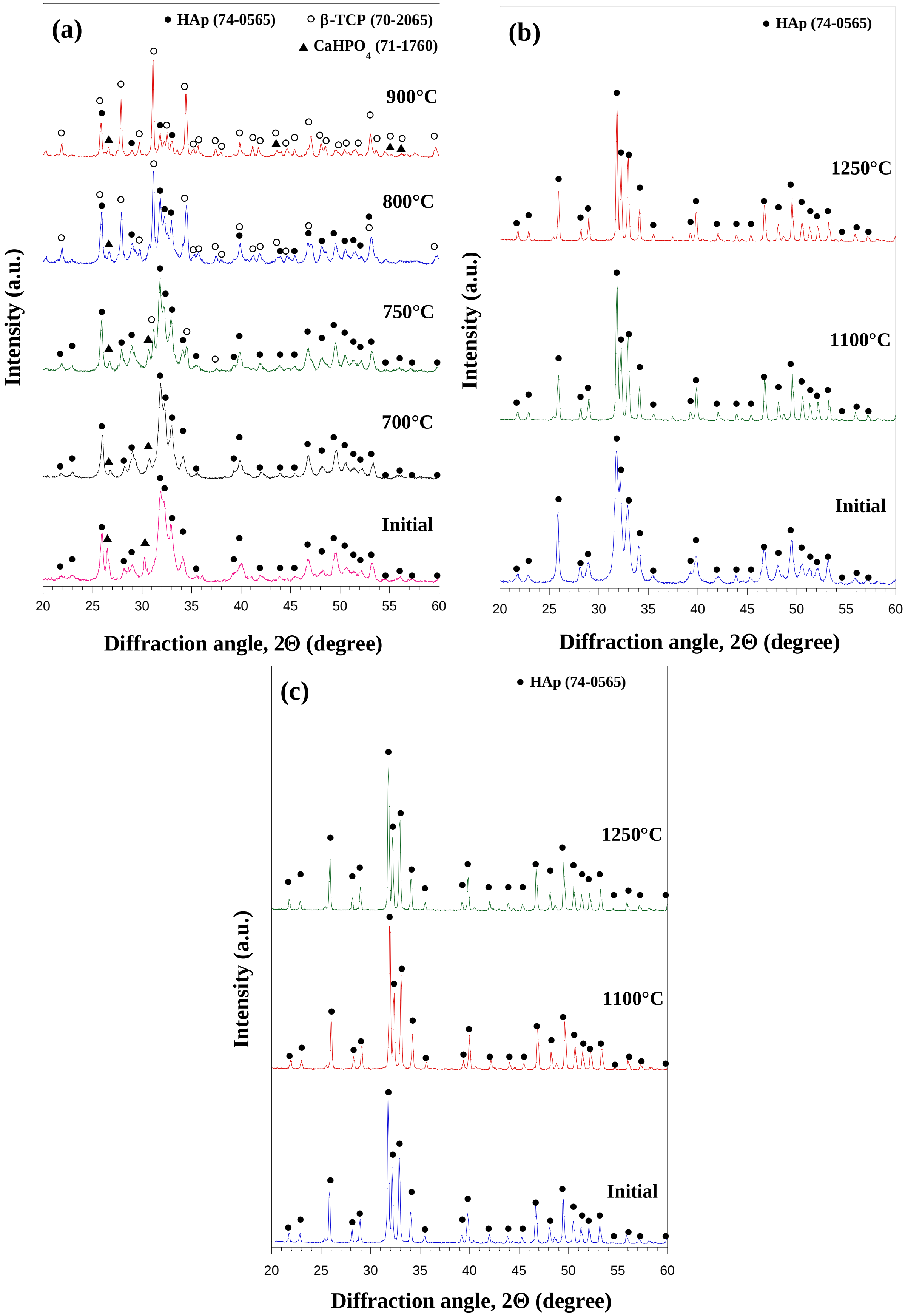

Figure 4. Mass loss of HAp powders during TGA in air.

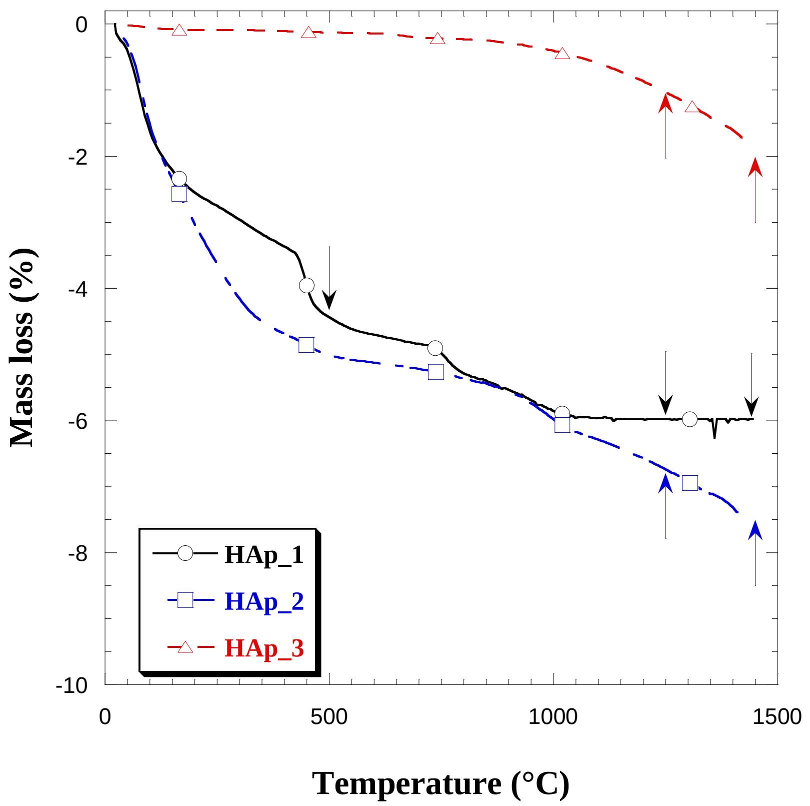

Figure 5. Compositional changes of (a) **HAp_1**, (b) **HAp_2** and (c) **HAp_3** powders during TGA (10°C/min) in air (100 ml/min) (cf. **Figure 4**).

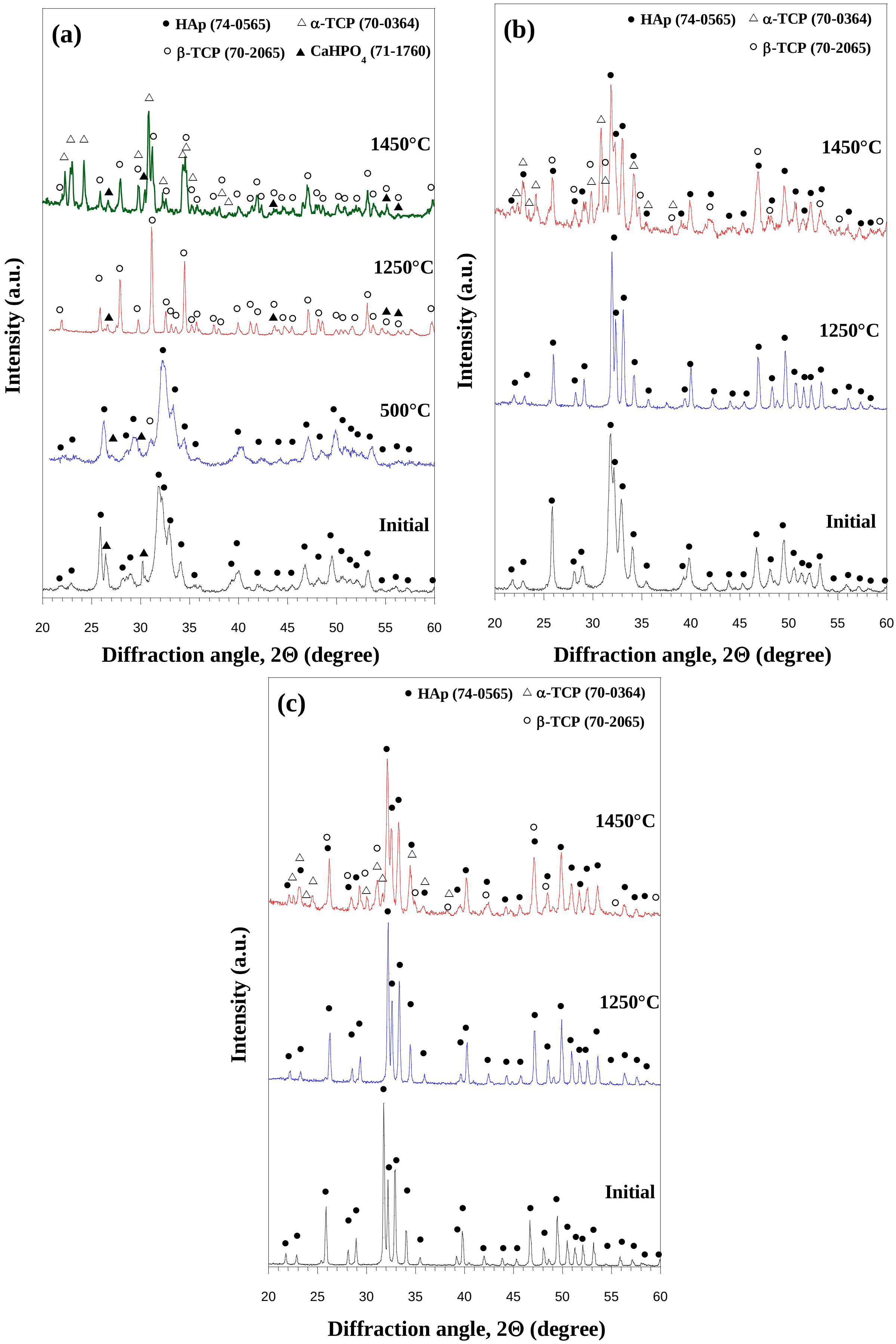

Figure 6. Temperature and sample shrinkage time profiles recorded during consolidation of **HAp_2** powders by SPS (900°C, 75 °C/min, t_D=5 min, 30 MPa).

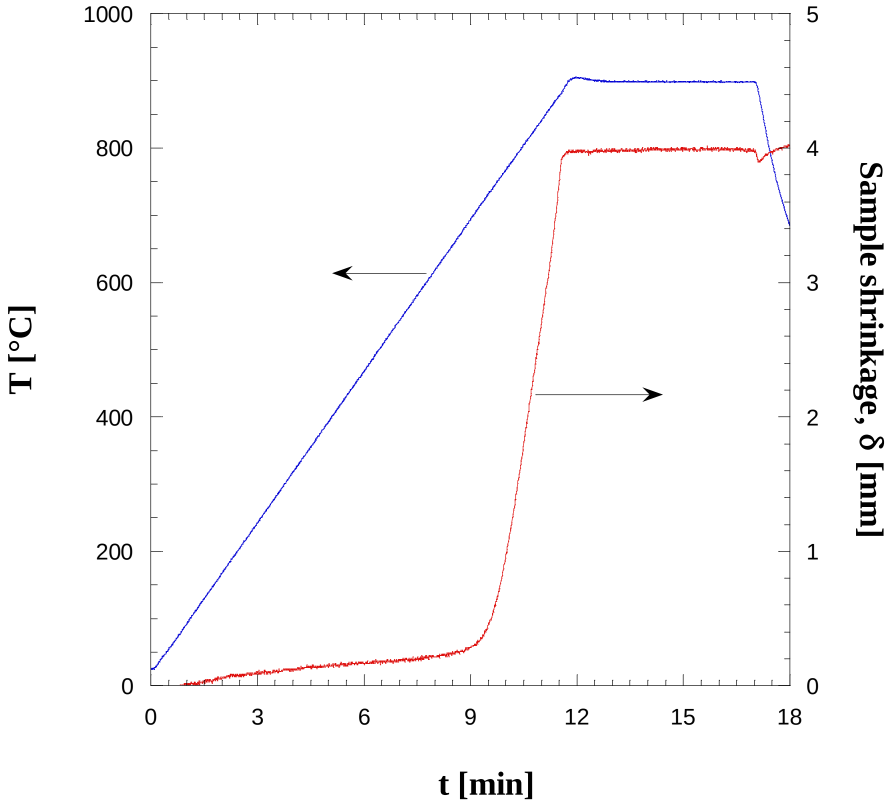

Figure 7. Influence of the sintering temperature on the density of the HAp products obtained by SPS (75 °C/min, t_D=5 min, 30 MPa).

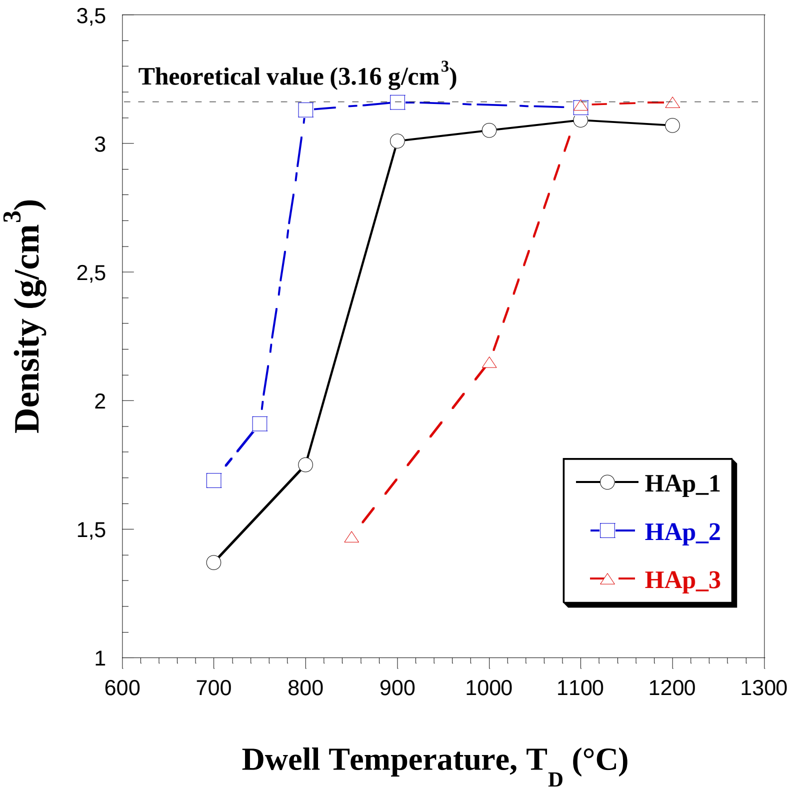

Figure 8. Comparison of XRD patterns before and after consolidation by SPS (75 °C/min, t_D=5 min, 30 MPa) of (a) **HAp_1**, (b) **HAp_2** and (c) **HAp_3** powders.

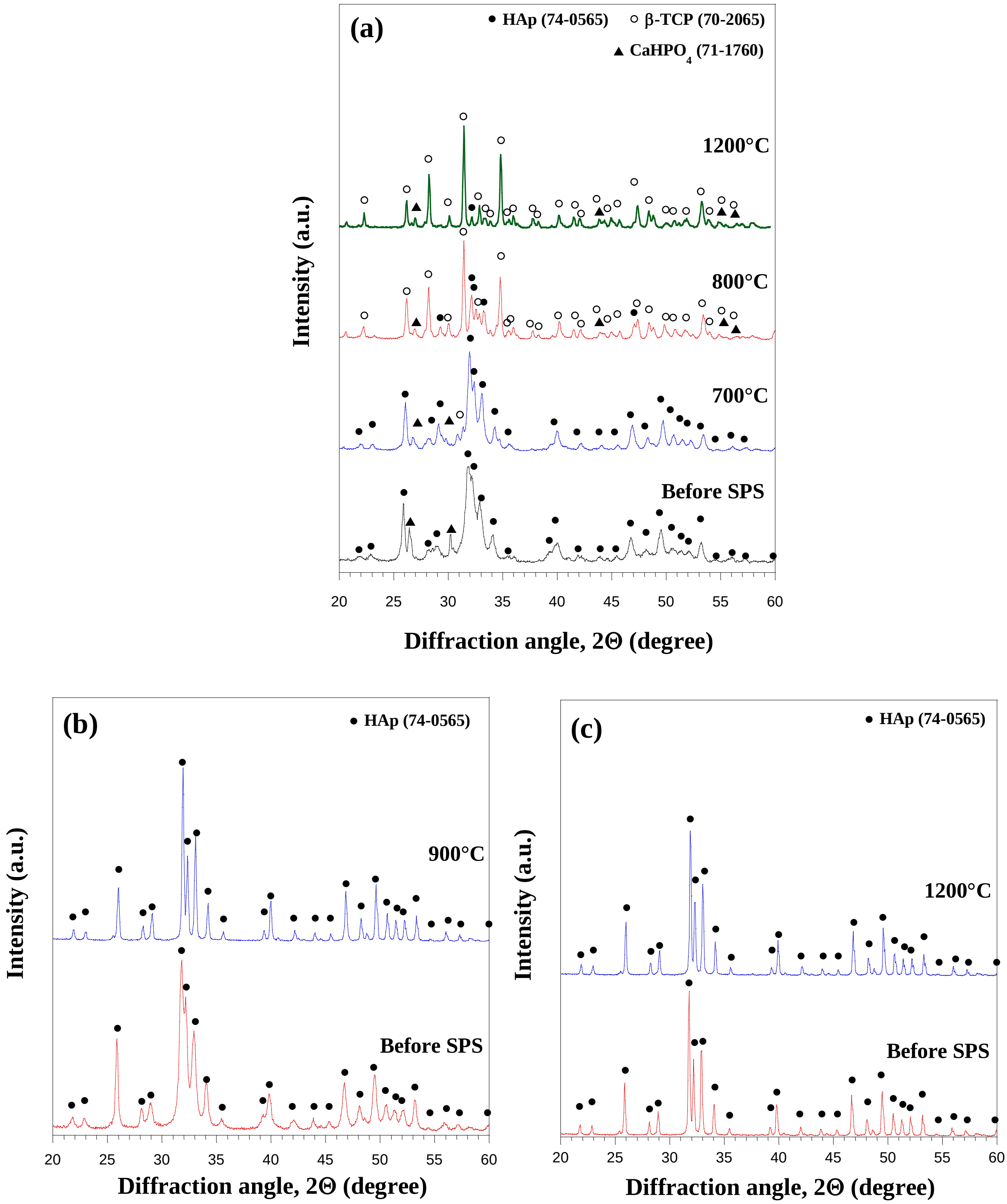

Figure 9. Temporal evolution of gas pressure during the SPS process (75 °C/min, t_D=5 min, 30 MPa) of **HAp_1**, **HAp_2** and **HAp_3** powders.

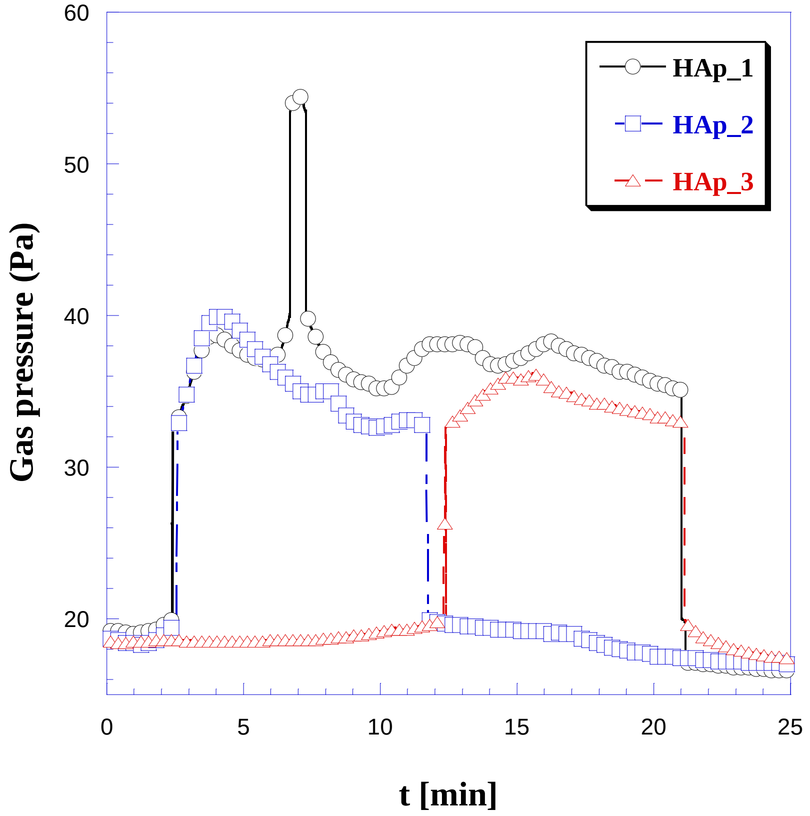

Figure 10. SEM micrographs (5000x) of chemically etched dense products obtained by SPS under optimal conditions: (a) **HAp_1**, (b) **HAp_2** and (c) **HAp_3**.

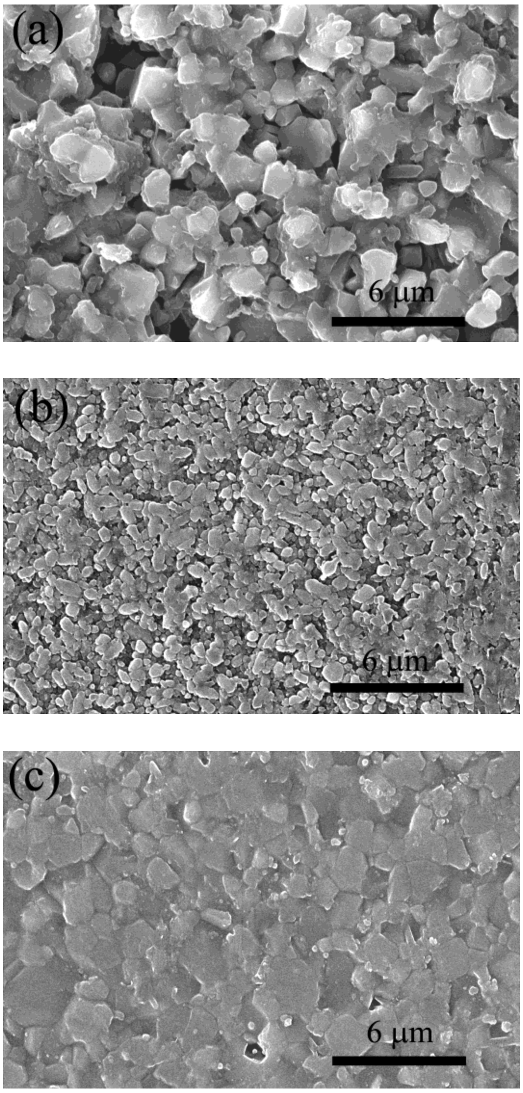

Figure 11. Optical photographs of dense products obtained by SPS under optimal conditions: (a) **HAp_1**, (b) **HAp_2** and (c) **HAp_3**.

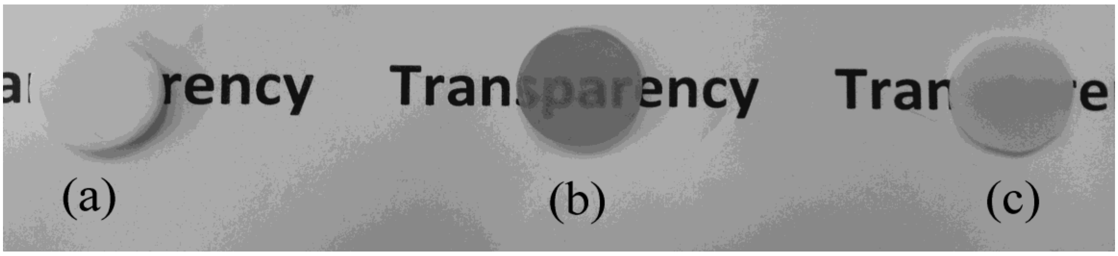

Figure 12. Residual imprints produced in the cross section of the **HAp_2** samples during indentation tests: (a) 0.5 N and 2.0 N (b) loads.

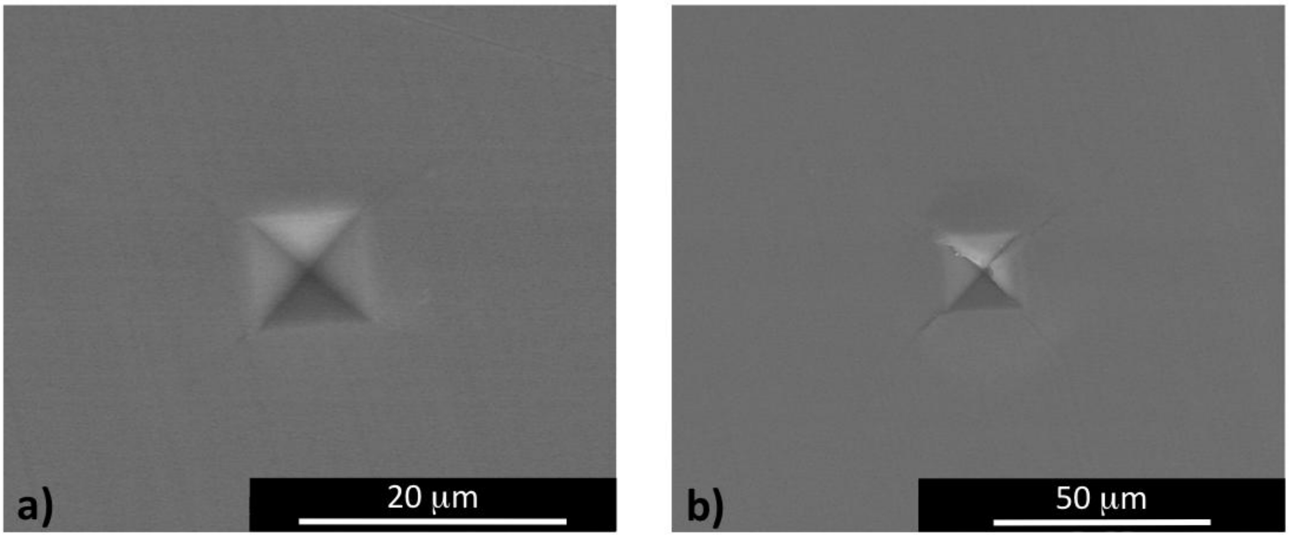

Figure 13. Mechanical test results performed on **HAp_1**, **HAp_2** and **HAp_3** materials obtained by SPS under optimal sintering conditions: (a) micro-hardness and (b) local elastic modulus.